



**NTNU – Trondheim**  
Norwegian University of  
Science and Technology

# The influence of using a ducted propeller on the motions and speed loss of a ship in waves

**Qi Pan**

Marine Technology

Submission date: June 2013

Supervisor: Sverre Steen, IMT

Co-supervisor: Anirban Bhattacharyya, IMT

Norwegian University of Science and Technology  
Department of Marine Technology



# **The influence of using a ducted propeller on motions and speed loss of a ship in waves**

Pan Qi

June, 2013

Master thesis

Department of Marine Technology

Norwegian University of Science and Technology

Supervisor: Professor Sverre Steen

Advisor: Anirban Bhattacharyya

## Abstract

Comparisons of experimental and numerical investigations into the effect of duct on motion variables and speed loss for a given ship model are presented. The purpose of these comparisons is to verify the advantage of using ducted propeller on sea keeping performance and added power or speed loss.

Relevant damping theories concerning the lift characteristic of ducts are described as foundation for the numerical calculations of using an equivalent flat plate that represents the duct of ducted propeller in software of SHIPX. In SHIPX, a case ship of RR NVC Nor-lines 120m cargo vessel is defined and several plug-in are used to do simulations for bare ship (refers to vessel with open propeller) and ship with foil (represents vessel with ducted propeller). The duct's effect on RAOs for motion variables, added resistance and speed loss are evaluated respectively under 5 different wave conditions.

A series of experiments on M3006 respectively with an open propeller and a ducted propeller are carried out in both calm water and 8 regular wave conditions in the large towing tank of MARINTEK center. Repetitions of tests under same wave conditions are used to make uncertainty analysis of measured variables. The effect of wave height and wave period affecting the duct's effect on motion variables and added resistance are discussed and compared with numerical results obtained from SHIPX.

Additionally, by interpolation of propeller rotational speed given tow rope force at self-propulsion point, corresponding thrust and torque are obtained. Then the interpolated variables are used to calculate propulsive coefficients including thrust deduction, wake fraction and relative rotative efficiency in both calm water and regular waves. The effect of wave height and wave period on propulsive coefficients are studied and compared for both open and ducted propeller. Furthermore, corrections are made for interpolation results to give more precise power prediction. The effect of propeller loading on wake fraction and propeller efficiency varying with 5 different wave conditions are presented. Finally the duct's effect on added power is studied and compared with numerical results from SHIPX.

---

# Preface

This is the master thesis of the author as part of International Master Study program for Department of Marine Technology at NTNU during the spring semester of 2013.

---

# Acknowledgments

The model tests performed in towing tank are sponsored by Rolls-Royce Marine through the UTC “performance in a seaway”, which is gratefully acknowledged.

The author would like to thank the following persons for their support and guidance with this master thesis:

Professor Sverre Steen: for all his wisdom, guidance and patience during not only different stages of the discussion about the thesis but also two hydrodynamic and a module courses he taught. His smart lectures with extensive knowledge were among best experiences at Tyholt campus.

Anirban Bhattacharyya: for all his assistance and support with SHIP-X involved with speed loss and powering for open and ducted propeller. He is not only advisor but also a good friend who shares the entire adventure.

People in my family who are thousands of miles away in China but still love me so much: for their unconditional love and support.

---

# Contents

Abstract.....	i
Preface.....	ii
Acknowledgments.....	iii
Contents .....	iv
List of Figures .....	vi
List of Tables.....	ix
Nomenclature.....	xi
1. Introduction.....	1
1.1 Background and motivation.....	1
1.2 Objectives and Scope of work .....	2
1.3 Approach.....	3
1.4 Literature survey .....	3
1.5 Structure of the thesis.....	4
2. Numerical calculations using SHIPX .....	5
2.1 Find equivalent flat plate size .....	5
2.1.1 Lift characteristics of the duct.....	5
2.1.2 Equivalent flat plate providing same lift force .....	7
2.2 SHIPX calculations .....	8
2.2.1 SHIPX vessel response .....	8
2.2.2 Ship speed and powering .....	16
3. Experimental calculation .....	19
3.1 General information about model tests .....	19
3.1.1 Model dimensions.....	19
3.1.2 Tests set up.....	20
3.1.3 Measurement.....	21
3.2 Wave calibration .....	21
3.3 Uncertainty and error analysis .....	24
3.4 The effect of duct on motions and accelerations.....	26
3.4.1 RAO for heave motion.....	26
3.4.2 RAO for pitch motion .....	28
3.4.3 RAO for acceleration in Z-direction .....	29
3.5 The duct's effect on added resistance .....	30
3.6 Analysis of propulsive factors change due to waves .....	34
3.6.1 Basic definition .....	34
3.6.2 Interpolation method.....	34
3.6.3 Calculation of propulsive factors .....	36
3.6.4 Observations from results and figures .....	41
3.7 The duct's effect on added power .....	42
3.8 The propeller's loading on wake fraction and propulsive efficiency.....	47

---

4. Comparisons of SHIPX and experimental results .....	50
4.1 RAO for motion variables.....	50
4.2 Non-dimensional added resistance .....	54
4.3 Augment of added power.....	55
5. Conclusion and further work .....	57
Reference .....	59
Appendix A: calculation of flat plate .....	61
Appendix B: numerical results from SHIPX .....	64
1. Ship response analysis .....	64
2. Added power and speed loss.....	64
Appendix C: calculation of tow rope force at self-propulsion point .....	67
Appendix D: calculation of propulsive factors .....	69



# List of Figures

Figure 2-1 Nozzle definition sketch (Taken from [13]).....	6
<b>Figure 2-2</b> Quasi-steady analyses of a heaving foil (Taken from [14]) .....	6
<b>Figure 2-3</b> Global coordinate system (3D) .....	9
<b>Figure 2-4</b> Global coordinate system (2D) .....	9
<b>Figure 2-5</b> View for flat plate in x-y plane.....	10
<b>Figure 2-6</b> Comparisons of RAO for heave motion at velocities .....	11
<b>Figure 2-7</b> Comparisons of RAO for pitch motion at velocities.....	11
<b>Figure 2-8</b> RAOs for vertical acceleration measured at AP for ducted propeller.....	12
<b>Figure 2-9</b> RAO for acceleration measured at AP for ducted propeller.....	12
<b>Figure 2-10</b> Comparisons of added resistance .....	13
<b>Figure 2-11</b> The duct's effect on RAO for heave .....	13
<b>Figure 2-12</b> The duct's effect on RAO for pitch .....	14
<b>Figure 2-13</b> The duct's effect on RAO for vertical acceleration measured at AP .....	14
<b>Figure 2-14</b> The duct's effect on RAO for vertical acceleration measured at FP .....	15
<b>Figure 2-15</b> The duct's effect on RAO for added resistance.....	15
<b>Figure 2-16</b> Comparisons of added power for open and ducted propeller at $F_n=0.2$ .....	17
<b>Figure 2-17</b> Comparisons of added power for open and ducted propeller at $F_n=0.14$ .....	17
<b>Figure 2-18</b> Comparisons of speed loss for open and ducted propeller.....	18
<b>Figure 2-19</b> The duct's effect on added power at $F_n=0.14$ and $F_n=0.20$ .....	18
<b>Figure 3-1</b> Experimental settings .....	20
<b>Figure 3-2</b> Model tested in the towing tank .....	20
<b>Figure 3-3</b> The positions of wave probes .....	20
<b>Figure 3-4</b> Energy spectrum of measured waves .....	22
<b>Figure 3-5</b> Measured wave during the test by wave probe .....	23
<b>Figure 3-6</b> Comparisons of RAO for heave motion at $F_n = 0.14$ and $F_n = 0.2$ .....	27
<b>Figure 3-7</b> The duct's effect on heave motion .....	27
<b>Figure 3-8</b> Comparisons of RAO for pitch motion at $F_n = 0.14$ and $F_n = 0.2$ .....	28
<b>Figure 3-9</b> The duct's effect on pitch motion.....	28
Figure 3-10 Comparisons of RAO for acceleration measure at FP .....	29
<b>Figure 3-11</b> Comparisons of RAO for acceleration measure at AP .....	29
<b>Figure 3-12</b> The duct's effect on vertical acceleration measured at FP .....	29
<b>Figure 3-13</b> The duct's effect on acceleration measured at AP .....	30
<b>Figure 3-14</b> Linear relationship between thrust and tow rope force for test 2001 .....	31
<b>Figure 3-15</b> Comparisons of added resistance for open and ducted propeller....	33

---

<b>Figure 3-16</b>	The duct's effect on added resistance.....	33
<b>Figure 3-17</b>	Read out RPS given tow rope force at self-propulsion point.....	35
<b>Figure 3-18</b>	Read out thrust given interpolated RPS at self-propulsion point....	35
<b>Figure 3-19</b>	Read out torque given interpolated RPS at self-propulsion point...	36
<b>Figure 3-20</b>	The effect of wave length on propulsive factors for open propeller at $Fn = 0.14$ .....	37
<b>Figure 3-21</b>	The effect of wave length on propulsive factors for ducted propeller at $Fn = 0.14$ .....	38
<b>Figure 3-22</b>	The effect of wave length on propulsive factors for open propeller at $Fn = 0.2$ .....	38
<b>Figure 3-23</b>	The effect of wave length on propulsive factors for ducted propeller at $Fn = 0.2$ .....	39
<b>Figure 3-24</b>	The effect of wave height on propulsive factors for open propeller at $Fn = 0.2$ .....	39
<b>Figure 3-25</b>	The effect of wave height on propulsive factors for ducted propeller at $Fn = 0.2$ .....	40
<b>Figure 3-26</b>	The effect of wave height on propulsive factors for open propeller at $Fn = 0.14$ .....	40
<b>Figure 3-27</b>	The effect of wave height on propulsive factors for ducted propeller at $Fn = 0.14$ .....	41
<b>Figure 3-28</b>	The effect of wave length on added power at $L/\zeta=130$ .....	44
<b>Figure 3-29</b>	The effect of wave length on interpolated results and corrected results at $Fn = 0.14$ .....	44
<b>Figure 3-30</b>	The effect of wave length on interpolated results and corrected results at $Fn = 0.20$ .....	45
<b>Figure 3-31</b>	The effect of wave height on interpolated results and corrected results at $Fn = 0.14$ .....	45
<b>Figure 3-32</b>	The effect of wave height on interpolated results and corrected results at $Fn = 0.20$ .....	46
<b>Figure 3-33</b>	The duct's effect on added power varying with wave periods.....	46
<b>Figure 3-34</b>	The duct's effect on added power varying with wave amplitude....	47
<b>Figure 3-35</b>	The effect of RPS on wake fractions varying with waves at $Fn = 0.14$ .....	48
<b>Figure 3-36</b>	The effect of propeller loading on propeller efficiency varying with waves.....	48
<b>Figure 4-1</b>	Comparisons of RAO for heave from SHIPX and experimental results with varying wave length at $Fn = 0.2$ .....	51
<b>Figure 4-2</b>	Comparisons of RAO for heave from SHIPX and experimental results with varying wave length at $Fn = 0.14$ .....	51
<b>Figure 4-3</b>	Comparisons of RAO for pitch from SHIPX and experimental results with varying wave length at $Fn = 0.20$ .....	51
<b>Figure 4-4</b>	Comparisons of RAO for pitch from SHIPX and experimental results with varying wave length at $Fn = 0.14$ .....	52
<b>Figure 4-5</b>	Comparisons of RAO for acceleration at FP from SHIPX and	

---

experimental results with varying wave length at $Fn = 0.20$ .....	52
<b>Figure 4-6</b> Comparisons of RAO for acceleration at FP from SHIPX and experimental results with varying wave length at $Fn = 0.14$ .....	52
<b>Figure 4-7</b> Comparisons of RAO for acceleration at AP from SHIPX and experimental results with varying wave length at $Fn = 0.20$ .....	53
<b>Figure 4-8</b> Comparisons of RAO for acceleration at AP from SHIPX and experimental results with varying wave length at $Fn = 0.14$ .....	53
<b>Figure 4-9</b> Comparisons of added resistance from SHIPX and experimental results with varying wave length at $Fn = 0.2$ .....	54
<b>Figure 4-10</b> Comparisons of added resistance from SHIPX and experimental results with varying wave length at $Fn = 0.2$ .....	54
<b>Figure 4-11</b> Comparisons of added power from SHIPX and interpolated experimental results with varying wave length at $Fn = 0.2$ .....	55
<b>Figure 4-12</b> Comparisons of added power from SHIPX and interpolated experimental results with varying wave length at $Fn = 0.2$ .....	55
<b>Figure 4-13</b> Comparisons of added power from SHIPX and experimental results by interpolated method and by final correction results with varying wave length at $Fn = 0.2$ .....	56
<b>Figure 4-14</b> Comparisons of added power from SHIPX and experimental results by interpolated method and by final correction results with varying wave length at $Fn = 0.14$ .....	56

---

## List of Tables

<b>Table 2.1</b>	The dimensions of flat plate.....	8
<b>Table 2.2</b>	Main dimensions for the vessel.....	9
<b>Table 2.3</b>	Propeller data .....	16
<b>Table 3.1</b>	Main dimensions of m3006 under loading conditions.....	19
<b>Table 3.2</b>	Data for the open propeller used in tests.....	19
<b>Table 3.3</b>	Data for the ducted propeller tested in experiments .....	19
<b>Table 3.4</b>	Target waves.....	21
<b>Table 3.5</b>	Calibrated waves compared with target waves .....	22
<b>Table 3.6</b>	Comparisons of calibrated waves with measured waves.....	23
<b>Table 3.7</b>	Measured results for four repetitions of tests.....	24
<b>Table 3.8</b>	Precision limit for one sample at 95% confidence estimate .....	25
<b>Table 3.9</b>	Precision limit for 4 samples at 95% confidence estimate .....	25
<b>Table 3.10</b>	Precision error .....	26
<b>Table 3.11</b>	Added resistance varying with wave conditions at $Fn = 0.14$ .....	31
<b>Table 3.12</b>	Added resistance varying with wave conditions at $Fn = 0.20$ .....	32
<b>Table 3.13</b>	The duct's effect on added resistance .....	32
<b>Table 3.14</b>	Tow rope force at self-propulsion point for two velocities .....	35
<b>Table 3.15</b>	Correction of added power due to deviation of tow rope force .....	43
<b>Table 4.1</b>	RAO definitions in SHIPX and in experimental results .....	50
<b>Table A.0.1</b>	Lift coefficient at three angles of attack [15] .....	61
<b>Table A.0.2</b>	Lift coefficient for aspect ratio of 1.05 [7] .....	61
<b>Table A.0.3</b>	Lift coefficient for aspect ratio of 2.....	61
<b>Table A.0.4</b>	Lift coefficients for flat plate with lift curve slop of 2.29 .....	62
<b>Table A.0.5</b>	Dimensions for flat plate based on resource 1.....	62
<b>Table A.0.6</b>	Lift coefficients for ring foil with $d/c$ ratio of 3.28.....	63
<b>Table A.0.7</b>	dimensions for flat plate based on model 2 .....	63
<b>Table B.0.1</b>	The duct's effect on motions and acceleration for 5 wave periods ..	64
<b>Table B.0.2</b>	The duct's effect on added resistance.....	64
<b>Table B.0.3</b>	Resistance data .....	65
<b>Table B.0.4</b>	Comparisons of added power for open propeller and ducted propeller .....	65
<b>Table B.0.5</b>	The duct's effect on added power varying with wave periods .....	65
<b>Table B.0.6</b>	The attainable speed for given brake power in calm water and in regular waves .....	66
<b>Table C.0.1</b>	The data for ship and model .....	68
<b>Table C.0.2</b>	Calculation of Reynolds number, frictional resistance coefficient and roughness allowance .....	68
<b>Table C.0.3</b>	Tow rope force at self-propulsion point .....	68
<b>Table D.0.1</b>	The results of interpolated propulsive factors for open propeller at $Fn = 0.14$ .....	69
<b>Table D.0.2</b>	The results of interpolated propulsive factors for ducted propeller at	

---

$F_n = 0.14$ .....	69
<b>Table D.0.3</b> The results of interpolated propulsive factors for ducted propeller at $F_n = 0.20$ .....	70
<b>Table D.0.4</b> The results of interpolated propulsive factors for open propeller at $F_n = 0.20$ .....	70
<b>Table D.0.5</b> The corrected results of propulsive factors at $F_n = 0.14$ .....	71
<b>Table D.0.6</b> The corrected results of propulsive factors at $F_n = 0.20$ .....	71

---

# Nomenclature

$a_{33}$	added mass coefficient of the vertical motion of a section $x_b$
$A$ ,	projected area of foil
$A_{duct}$	projected area of duct
$A_{flat}$	projected area of flat plate
$b_{33}$	damping coefficient of the vertical motion of a section $x_b$
$B$	breadth of the ship
$B_{33}$	damping coefficient in heave due to foil lift
$c$	chord length of foil
$C_{LN}$	lift coefficient
$C_T, C_{TH}$	propeller thrust coefficient
$C_{YN}$	nozzle cross force coefficient
$d, D_N$	diameter of duct
$d_{duct}$	diameter of the duct
$d_{prop}$	propeller diameter
$E_x$	precision errors for one sample
$E_{\bar{x}}$	precision errors for four samples
$F_D$	tow rope force
$h$	relative vertical motion between foil and incident waves
$H_D$	target wave height
$H_M$	wave height measured during the tests
$J$	advance ratio
$K_T$	thrust coefficient
$K_Q$	torque coefficient
$L$	ship length
$L_N$	lift force induced by propeller on the duct
$N$	numbers of repetition
$P$	power
$P_D$	deliver power

---

$P_E$	effective power
$P_X$	precision limit for one sample
$P_{\bar{X}}$	average precision limit of N samples
$\Delta P_{duct}\%$	the degree of added power augment due to the duct (see <i>Equation (2.15)</i> )
$\Delta P_{D\_change}$	the deviation of delivered power due to change of self-propulsive point
$R_{AW}$	added resistance due to waves
RPS	propeller rotational speed (round per second)
S	projected area
$t$	thrust deduction fraction
$t_0$	interval range for variables
$T$	thrust for the propeller system
$T_D$	designed wave period
$T_M$	calibrated wave period
$T_{prop}$	propeller thrust
$T_{tot}$	total thrust
$u_m$	mean velocity induced by propeller on the duct
U	incident wave velocity
$U_{RZ}$	the average relative vertical velocity in heave
$v$	incoming velocity to steering nozzle
V	ambient velocity (total velocity), ship speed
$v_a$	advance speed
$\Delta V_{duct}\%$	the degree of change of speed loss due to the duct (see <i>Equation (2.16)</i> ).
Z	propeller blade number
$w_p$	potential wake
$w$	effective wake, general wake fraction
$\eta$	general representative for heave, pitch, acceleration and added resistance
$\eta_3$	heave motion of foil/ship
$\Delta\eta_{duct}\%$	the degree of deviation of variables between open and ducted propeller, see <i>Equation (2.14)</i>
$\dot{\eta}_3$	vessel vertical velocity
$\ddot{\eta}_3$	vertical acceleration
$\eta_5$	pitch angel
$\eta_R$	relative rotative efficiency
$\eta_0$	propeller efficiency

---

$\eta_H$	hull efficiency
$\eta_D$	quasi-propulsive efficiency
$\lambda$	wave length
$\zeta'$	effective wave displacement for a cross section
$\zeta_r$	relative wave amplitude along the ship
$\omega$	encounter frequency
$\omega_n$	circular wave frequency
$\delta$	small angle of attack
$\rho$	fluid density
$\alpha$	instantaneous angle of attack
$\nabla$	volume displacement
$\zeta$	wave amplitude of regular waves
$\mu$	mean value of variables
$\sigma$	standard deviation of variables
$\gamma$	confidence interval



# 1. Introduction

## 1.1 Background and motivation

Ducted propellers sometimes are called Kort nozzles, including two principal components: an annular duct which has an aero-foil cross section and the propeller applicable to the duct [1].

The first studies by Stipa and Kort in 1930s showed the benefits of ducted propeller [2]. Using accelerating duct around the propeller can easily increase propulsion efficiency by reducing axial losses. Ducted propeller can save up 20% when providing energy [3]. And ducted propellers have been applied to cases where high thrust at low speed is preferred, for instance, in towing and trawling situations. In these cases, the duct can make contribution 50% of the total thrust as propulsor under the bollard pull condition [1].

Although the statements presented the advantage of ducted propellers, few evidence of validity has been found to support the favor of using a ducted propeller on reducing the ship motions and increasing ship's speed. Reliable evaluation of ducted propeller is essential for proper design and optimizations for ships. For this purpose, model tests and numerical calculations of a ship with both a ducted propeller and an open propeller were carried out to give evidence of the duct's influence on ship's performance, in particular on ship's motions and powering.

Currently the decision of choosing a ducted propeller or open propeller is made based on the assessment of performance in calm water. However, due to changing wave fields the hydrodynamic forces (or moments) which both the ship and the propeller bear are changing with time. It is, therefore, necessary to investigate the ship's motion, forces and propulsion characteristics in waves in order to present power prediction in real sea states [4].

Furthermore, it is claimed that empirically the wake fraction will reduce in waves, however, the discussion of the change of propulsive factors in waves is too little for open propeller and non for ducted propeller. Variation of propulsive factors in waves is very important, particularly when wave's frequency closes to natural frequencies of ship motions, such as heave and pitch [5].

Hence, it is necessary to give detailed studies about propulsive factors in waves for better predictions of added power in rough sea states.

---

## 1.2 Objectives and Scope of work

There are three main objectives of this thesis:

1. To evaluate the effect of the duct on ship's motions and accelerations and added resistance in waves.
2. To assess the influence of duct on added power changing with wave conditions.
3. To investigate the characteristics of the propulsive factors varying with wave conditions and the difference between the results of using a ducted propeller and an open propeller.

This thesis studies the waves' influence on the performance of a ducted propeller compared with an open propeller on ship's motion and power prediction. Numerical calculations in SHIPX aim to give first estimations of the duct's effect on ship's motions and speed loss (added power) in waves. Then the experimental results of model tests conducted in large towing tank of MARINETEK are made analysis to present more accurate tendency of duct's effect. Additionally, based on experimental results, the change of propulsive factors with wave conditions for both a ducted propeller and an open propeller are discussed and compared.

The scope of this thesis is summarized as follows:

1. Estimation of area of an equivalent flat plate representing the duct to provide same lift force and numerical calculations in SHIP-X. A RR NVC Nor-lines 120[m] cargo vessel was defined and plug-in of SHIP-X were used to simulate vessel response and power prediction for case vessel with an open propeller and a ducted propeller. RAOs for motion and force variables, added resistance, and predicted brake power are obtained.
2. Analysis of experimental results to show the duct's effect on ship's motion and force variables including heave, pitch, vertical acceleration as well as added resistance and added power in waves. Uncertainty analysis is made .And the interpolated method is applied to find force and motion variables for open and ducted propeller at self-propulsion point.
3. Analysis of propulsive factor in waves and difference of results between an open propeller and a duct propeller. The effect of propeller loading on wake fraction and quasi-propulsive coefficient are investigated.
4. Comparisons of numerical and experimental results to evaluate the waves' influence on ship's motion and powering performance and to give evidence for advantage of using a ducted propeller on sea-keeping and added-power.

---

## 1.3 Approach

The tools used are: numerical calculations in SHIPX and model tests performed in the towing tank of MARINTEK.

For numerical calculations in SHIPX, plug-in called vessel responses and ship speed and powering were used to run simulations for bare hull (refers to ship with an open propeller) and ship with foil (represents ship with a ducted propeller). By comparisons of different RAO values for heave, pitch and added-resistance, duct's effect on ship's motion were evaluated. By conducting speed and powering analysis with resistance at different wave periods, speed loss due to added resistance in waves and extra power to maintain designed speed were obtained.

As for experiments tested in towing tank, model was first installed with ducted propeller and then open propeller in both calm water and regular waves. Variables including wave, speed of carriage, speed of propeller, motion variables (heave, pitch, accelerations) and forces variables (torque and thrust of open propeller or ducted propeller) were recorded as time series. Resistance for each wave condition was interpolated from the linear curve of tow rope force as a function of thrust. Added resistance or added power was calculated as difference of mean resistance or power in calm water and regular waves. Propulsive factors (thrust deduction, wake fraction and relative rotative efficiency) were calculated based on their definition using the interpolated method.

## 1.4 Literature survey

The sea-keeping performances of most merchant ships are connected with capability to maintain designed speed in rough sea states [6]. There is lack of work about duct's effect on speed loss. Early studies of ducted propeller before 1960s focus on investigations in geometrical changes of duct in static or uniform flow conditions. Relatively few investigators did experimental researches on pressure and velocity distribution of the ducted propeller, neither clear relationship between flow and duct's performance were found [2].

Morgan and Caster [7] showed the details of pressure and velocities distributions on the ducts for different angles of attack and chord-diameter ratio. A series of model tests on decelerating ducted propellers with different nozzle shapes operating at same thrust coefficient were performed to prevent the occurrence of cavitation. The ideal efficiency of a ducted propeller will decrease with increasing ratio of propeller thrust over total thrust [8].

Previous considerations only limited to interaction between duct and propeller. Later

---

studies on ducted propeller involved the interaction between ducted propeller and hull especially with help of development of computer technology, more precise analysis were made. Falcao de Campos [9] found important effects on the performance of ducted propellers in uniform and non-uniform axisymmetric flows. Approximate numerical solutions of Euler's equation are demonstrated and applied to the interaction studies between a ducted propeller and the stern for axisymmetric flows. Barros and Dantas [10] evaluated the duct effect on maneuverability for AUV using CFD simulation for modeling the flow around a propeller duct at different angles of attack. Also the interaction between the duct and the bare hull wake is investigated by comparing results of predictions based on CFD, ASE and on the combination of both approaches with experimental results in a towing tank.

Generally the ducted propellers were installed behind the hull in the wake of ship where the flow region was not uniform. The reasons for variation of propulsive efficiency in a seaway are as followed:

1. Increased propeller loading ;
2. Interference between propeller and water surface;
3. Propeller out of water;
4. Changes in boundary layers and propeller wake due to waves. [6]

Propulsion analysis in waves including the change of thrust deduction, wake fraction as well as relative rotative efficiency were paid extensive attention by Nakamura and Natio [4], Faltinsen and Minsaas [5]. In addition, the changing propulsive efficiency due to change of propulsion point in waves for certain stem shapes were analyzed by Chuang and Steen [11].

## **1.5 Structure of the thesis**

This paper is divided into five main chapters. The first one introduces general information about thesis. Chapter2 deals with numerical calculations in SHIP-X using an equivalent flat plate to replacing the duct and discusses numerical results on RAO for motion and force variables, added resistance, and added power under different wave conditions for both open and ducted propeller. Details about model tests are shown in Chapter 3 and experimental results are analyzed to give general conclusions about duct's effect and change of propulsive factors due to waves. The effect of propeller loading on effective wake fraction and quasi-propulsive coefficient is discussed. Comparisons of numerical and experimental results are considered in Chapter 4. Conclusions and recommendation for further work are presented in Chapter5.

## 2. Numerical calculations using SHIPX

SHIPX is MARINTEK's design and analysis tool for assessing ship hydrodynamic performance. Mainly functionality in SHIPX is so-called Plug-Ins. Important SHIPX Plug-Ins include: vessel responses, ship speed and powering, station keeping, maneuvering and so on [12].

There is no selection of applying a ducted propeller in vessel response calculation; therefore, it is needed to first find an equivalent model that would represent the duct in the SHIPX simulations.

### 2.1 Find equivalent flat plate size

Instead of directly using the duct as input in SHIPX Vessel Response Program, a flat plate is applied in SHIPX to replace annular foil as representative for the duct to provide same lift force as the duct. It is necessary to start from theoretical lift characteristics of the duct.

#### 2.1.1 Lift characteristics of the duct

The duct can be modeled as a steering nozzle which is preferable to apply at highly loaded propeller of tugs, watercraft and research vessels [13]. The ducts of these ducted propellers are not being fixed to the hull but found to be steerable.

For steering, it means that the duct is allowed to rotate about the axes, thus the thrust of the propeller can be adjust to a desired direction [1].

The geometrical model is shown as **Figure 2-1**. The lift force and induced drag are based on linear foil theory in steady states with small angle of attack, and the lift force is expressed as

$$L_N = \frac{\pi}{2} \rho v^2 c_N D_N \left(1 + \frac{u_m}{v}\right)^2 \left(\frac{dC_L}{d\delta}\right) \delta \quad (2.1)$$

And

$$\left(1 + \frac{u_m}{v}\right)^2 \left(\frac{dC_L}{d\delta}\right) = \frac{C_{YN}}{\delta} \left(\frac{c_N}{D_N}, C_{TH}\right) \quad (2.2)$$

where  $u_m$  refers to the mean velocity induced by propeller on the duct and depends on the propeller thrust loading coefficient  $C_{TH}$  and chord-diameter ratio  $\frac{c_N}{D_N}$ ;  $C_{YN}$  is nozzle cross force coefficient.

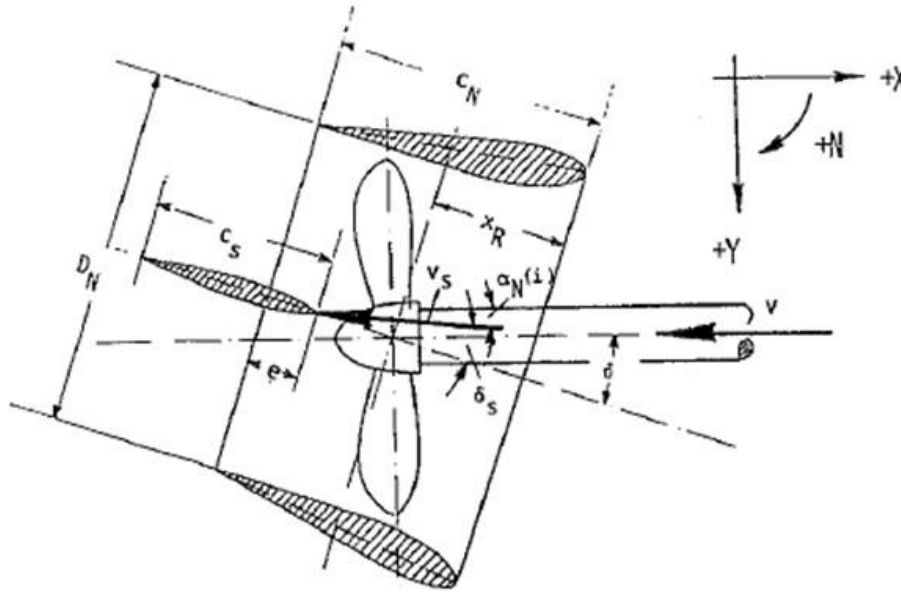


**Figure 2-1** Nozzle definition sketch (Taken from [13])

For small angle of attack, steering force approximately equals to lift force. Thus, the lift force can be written in terms of  $C_{YN}$  as:

$$L_N = \frac{\pi}{2} \rho v^2 c_N D_N \delta \left( \frac{C_{YN}}{\delta} \right) \quad (2.3)$$

Assume a heaving foil with no camber and zero angle of attack moving with forward velocity in 2D infinite flow. For quasi-steady analysis, the incident waves travel with velocity  $U$  parallel to the foil and induced velocity  $\frac{-d\eta_3}{dt}$  normal to the foil. See **Figure 2-2**. Here  $\eta_3$  is the heave motion of foil;  $h$  is the relative vertical motion between foil and incident waves.

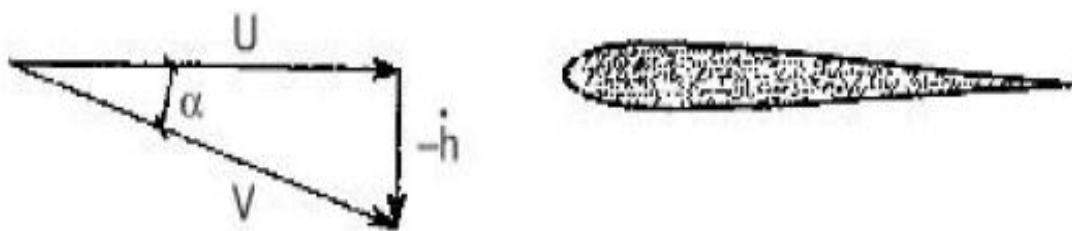


**Figure 2-2** Quasi-steady analyses of a heaving foil (Taken from [14])

If only heave motion is considered, the total velocity would be:

$$V = \sqrt{U^2 + \left( \frac{d\eta_3}{dt} \right)^2} \quad (2.4)$$

So relative to the foil comes the instantaneous angle of attack:

$$\alpha = \frac{-\frac{d\eta_3}{dt}}{U} \quad (2.5)$$

Consider quasi-steady conditions, we can get lift force (per length unit) for flat plate expressed as:

$$L = 0.5\rho U^2 c(2\pi\alpha) = -\rho U c \pi \frac{d\eta_3}{dt} \quad (2.6)$$

where  $c$  is the chord length. According to motion equations, damping force equals to product of damping coefficient and motion velocity.

So the damping coefficient in heave due to foil lift is written as:

$$B_{33}^{2D} = \rho U c \pi \quad (2.7)$$

Expanded for general cases with unsteady flow variations, damping coefficient of the unsteady part of lift force can be shown as:

$$B_{33}^L = 0.5\rho U^2 A \frac{dC_L}{d\alpha} \quad (2.8)$$

By linking the lift force with foil-lift damping terms of duct, it is found that projected area (product of chord and diameter) and slope of steering force (or lift force) over angle of attack determine the lift coefficient.

### 2.1.2 Equivalent flat plate providing same lift force

Annular airfoil can be used to represent duct based on three independent sources [7] [15] [16] and to give separately lift curves in expression of lift angles. Since tip clearance and thickness of ducted propeller were neglected, diameter of the duct equals the propeller diameter. Aspect ratio of duct (duct diameter over for length of duct) was set 2 in this thesis. This value is also chosen in ducted propeller design by Celik, Guner and Ekinici [3]. Thus length of duct becomes 2.1 [m] and projected area of duct equals 8.82 [m<sup>2</sup>].

Providing identical lift force, the area of flat plate has certain relationship with the projected area of duct:

$$C_{Lplate} A_{plate} = C_{Lduct} A_{duct} \quad (2.9)$$

The details of finding the area of equivalent flat plate are described in Appendix A. Two methods agree with each other and average projected area for two models which equals 20.11[m<sup>2</sup>] is chosen as the area for flat plate to be calculated in SHIPX, thus the corresponding length of span is 6.34[m] and length of chord is 3.17[m].

However some corrections are required for the projected area of flat plate, since two methods consider lift induced only from the duct rather from the ducted propeller as a whole. So contribution from existence of propeller should be added to get total lift force, that is

$$C_{Lduct} + \Delta C_{Lporp} = C_{Ltotal} \quad (2.10)$$

where  $C_{Lduct}$  indicates lift force only from duct,  $C_{Ltotal}$  represents lift provided by

ducted propeller. So the corrected projected area relationship between the ducted propeller and flat plate should be written as

$$(C_{Lduct} + \Delta C_{Lporp}) \times A_{duct} = \frac{1}{2} C_{Lduct} \times A_{plate} \quad (2.11)$$

$$A_{plate} = 2 \times \left(1 + \frac{\Delta C_{Lporp}}{C_{Lduct}}\right) \times A_{duct} \quad (2.12)$$

Based on thrust tests of ducted propeller with duct's aspect ratio of 2, lift coefficient of the ducted propeller is function of thrust coefficient within ( $0.26 < C_{TH} < 9$ ).

$$C_{Ltotal} = 0.0024 \times C_{TH}^2 - 0.0401 \times C_{TH} - 0.0551 \quad (2.13)$$

Given  $C_{TH} = 1.35$ ,  $C_{Ltotal} = 0.106$ , using method2 the lift coefficient for duct  $C_{Lduct} = 0.08$ .

By applying equation (2.12), it gives the area of flat plate as 22.18 [m<sup>2</sup>]. It is 10.29 % higher than previous 20.11 [m<sup>2</sup>]. And the dimensions for calculated flat plate are list as **Table 2.1**.

**Table 2.1** The dimensions of flat plate

Length of span [m]	6.66
Length of chord [m]	3.33
Projected area [m <sup>2</sup> ]	22.18

## 2.2 SHIPX calculations

For numerical calculations, a RR NVC Nor-lines 120[m] cargo vessel was defined and plug-in of SHIP-X were used to do simulations for motions and forces of both ship with open propeller and ship with ducted propeller.

### 2.2.1 SHIPX vessel response

First the case vessel should be defined. A RR NVC Nor-Lines 120m Cargo Vessel is used in the calculation and basic information for the ship is given as

**Table 2.2.**

SHIPX vessel response was applied to solve the equations for wave effects on case ship. After importing hull lines and setting loading conditions, the global coordinates system used for this analysis are shown as **Figure 2-3** and **Figure 2-4**.

The global coordinate system is a right-handed Cartesian coordinate system with its origin at bottom line and positive z-direction upwards. The calculation method is selected as standard 2D strip theory, and the radii of gyration are given 4.5[m] relative



to the center of gravity.

**Table 2.2** Main dimensions for the vessel

variable	Symbol and unit	value
Length between perpendiculars	$L_{PP}$ [m]	117.600
Length on waterline	$LWL$ [m]	119.190
Breadth molded	$B$ [m]	20.800
Mean draught	$T$ [m]	5.500
Volume displacement	$\nabla$ [m <sup>3</sup> ]	7320

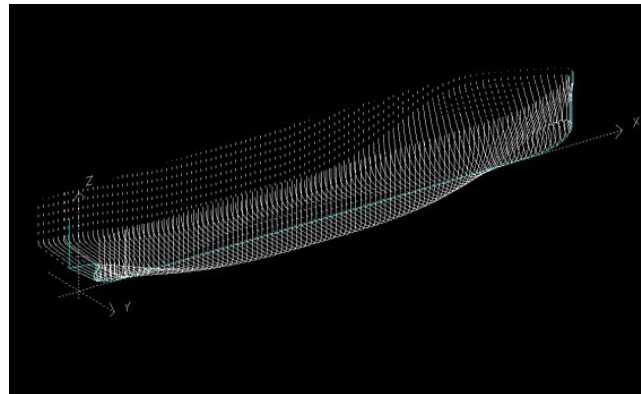


**Figure 2-3** Global coordinate system (3D)

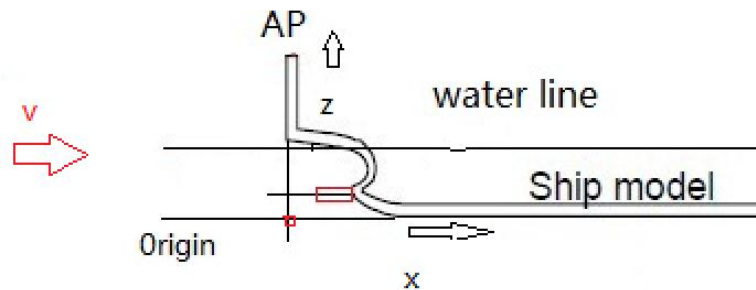


**Figure 2-4** Global coordinate system (2D)

Reading from hull geometry of case ship, shaft centerline of the ducted propeller locates 3.48[m] positive in x-direction and 2.34[m] above the bottom line. In addition, position of flat plate in y-direction is required as user input. This is defined by setting values for inner tip and outer tip of the flat plate. Based on dimensions of calculated foil, the input should be 3.33 for y-direction. See **Figure 2-5**.

Edit foil pair no. 1:

Position of foil and chord length:

	Inner tip	Outer tip	
Longitudinal position :	1.500	1.500	(m) rel. AP
Transverse position:	0.000	3.330	(m) rel. to centerline
Vertical position:	2.000	2.000	(m) above Base Line
Chord length:	3.330	3.330	(m)

Lift coefficient:

Calculate lift slope coefficient from foil geometry (no mirror effects assumed)

Lift slope coefficient (if not calculated): 2.292 (1/rad)

Controller coefficients:

Control on vertical motions Specify... Max. working angle to each side: 20.000 (deg.)

Control on relative vertical motions Specify... Overall effectiveness factor: 1.000 (-)

Control on roll motions Specify... Flap effectiveness factor (kappa): 1.000 (-)

Control on pitch motions Specify... The flap eff. factor should be 1.0 if the whole foil is being controlled. If the foil has a flap which covers parts of the chord length, the value should be less than 1.0.

Control on yaw motions Specify...

The input here describes the starboard foil, a corresponding foil will be applied on the port side of the vessel.

**Figure 2-5** View for flat plate in x-y plane

The wave conditions were defined in the condition information dialog with six wave periods of 6.44, 7.76, 8.68, 9.50, 10.63 and 11.96 [s]. The default wave height is 1[m]. In order to be more precise for power prediction, a large range of velocities is included from 7 to 16 [knot].

After wave response calculation, post processing should be undertaken for plotting results from SHIPX vessel response. SHIPX gives non-dimensional results as transfer functions, which are proportion of wave amplitude or wave slope “transferred” by the ship “system” into the ship motions [12].

For calculation of added resistance the method of pressure integration is selected.

The results for ship motion and added resistance in non-dimensional form with varying wave periods are listed in **Figure 2-6**, **Figure 2-7**, **Figure 2-8**, **Figure 2-9** and **Figure 2-10**.

In order to study the effect of presence of duct on motions and added resistance of the model, the deviation of RAO between results of model with open propeller and with ducted propeller is calculated and drawn into figures from **Figure 2-11** to **Figure 2-15**. For more details see *Appendix B*.

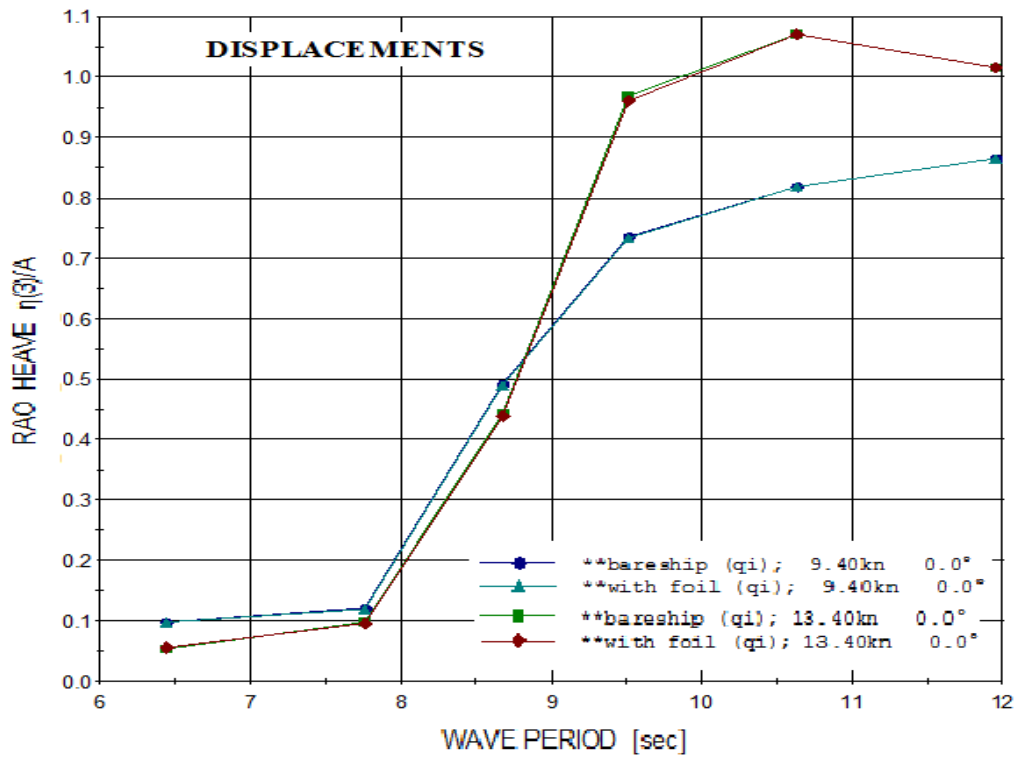


**Figure 2-6** Comparisons of RAO for heave motion at velocities

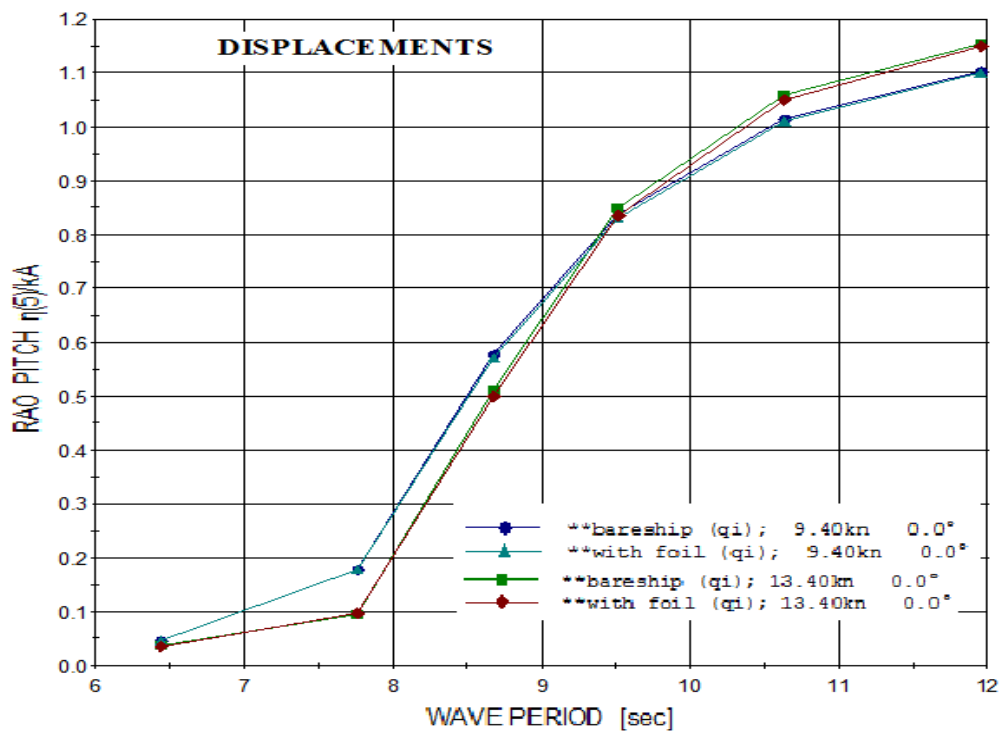


**Figure 2-7** Comparisons of RAO for pitch motion at velocities

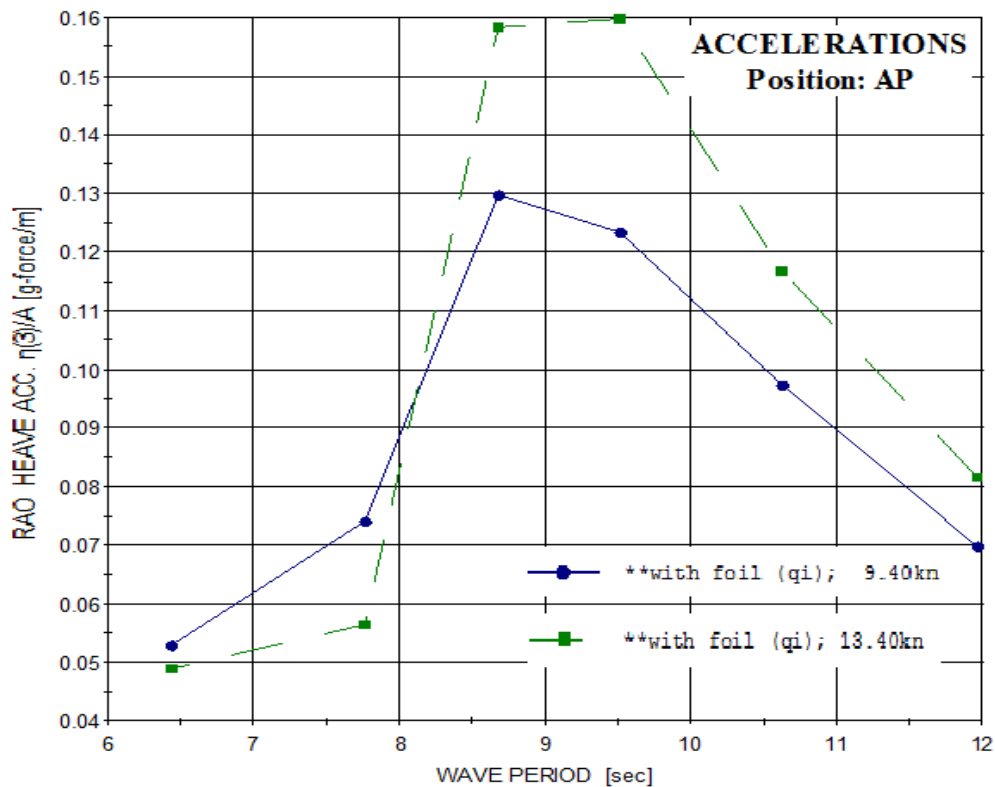


**Figure 2-8** RAOs for vertical acceleration measured at AP for ducted propeller

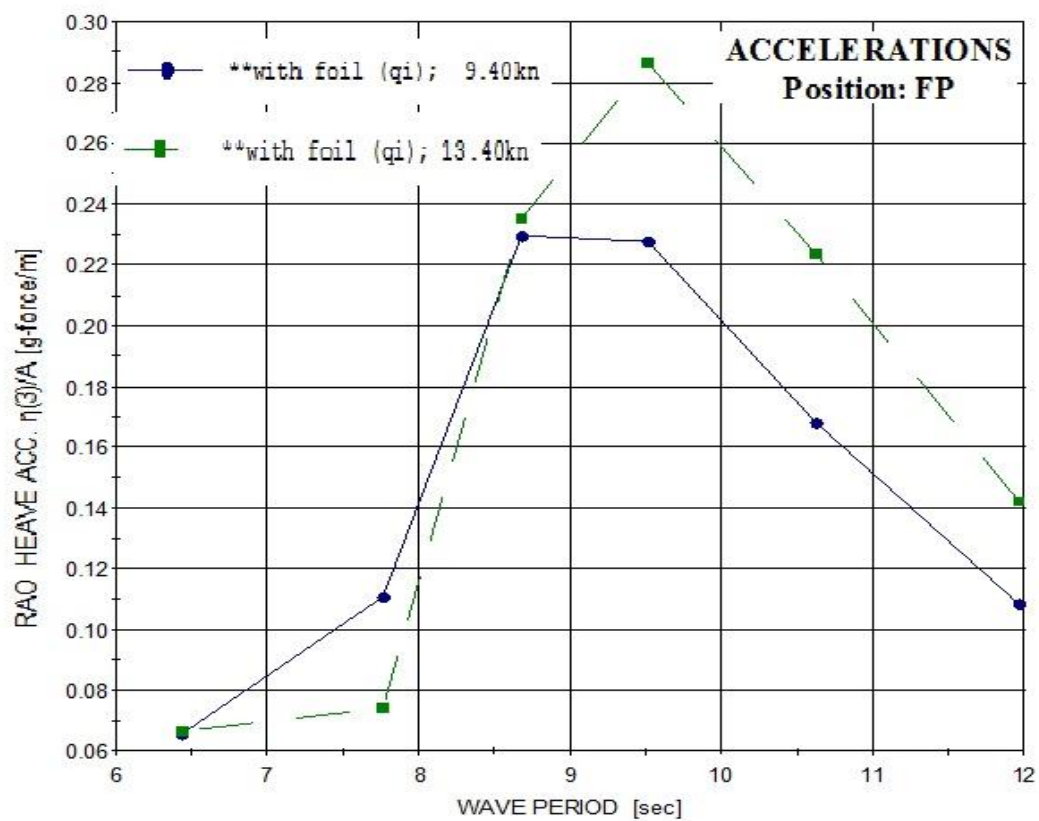


**Figure 2-9** RAO for acceleration measured at AP for ducted propeller

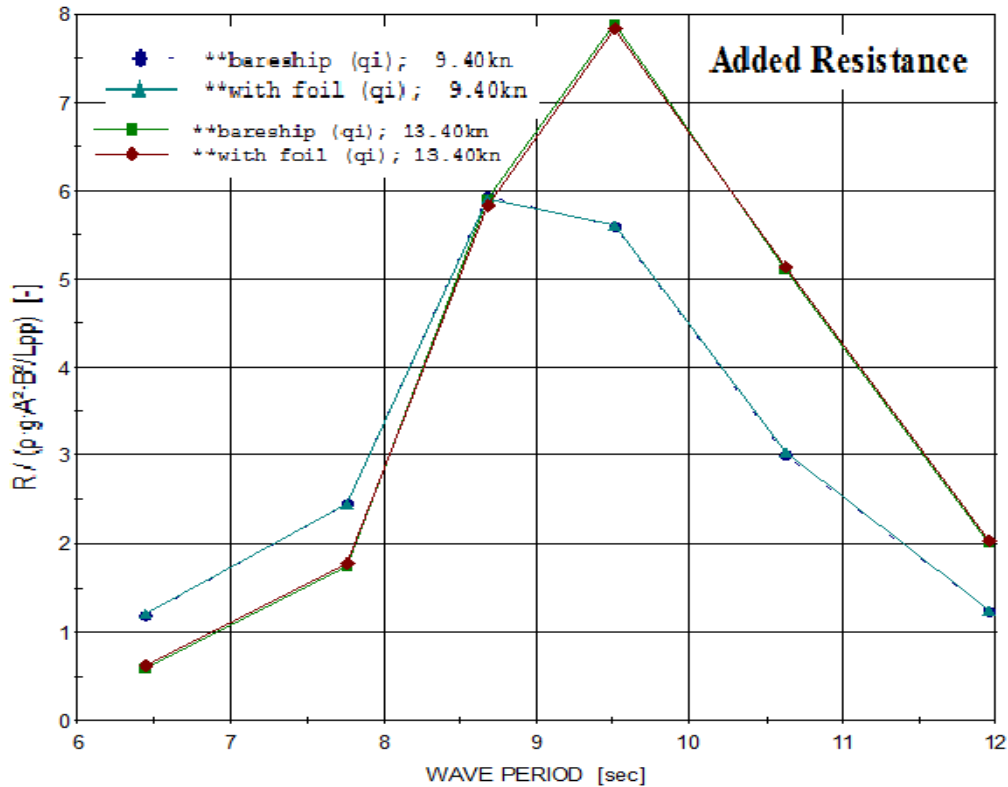


Figure 2-10 Comparisons of added resistance

The deviation of RAO for motion and added resistance between open propeller and ducted propeller are calculated as Equation (2.14)

$$\Delta\eta_{duct} \% = \frac{\eta_{duct} - \eta_{open}}{\eta_{open}} \times 100\% \tag{2.14}$$

Here  $\eta$  represents the ship motion variables for heave, pitch and vertical accelerations as well as added resistance.

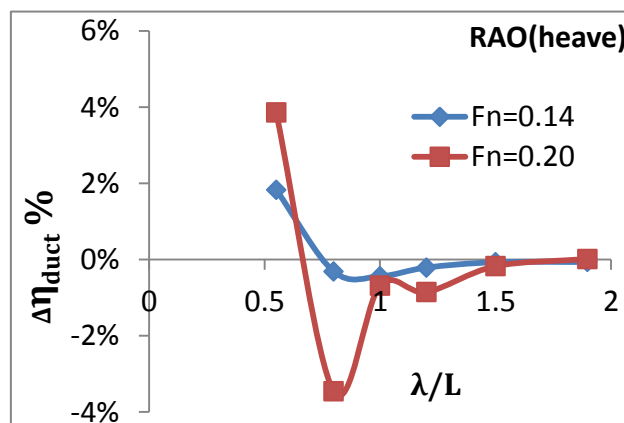
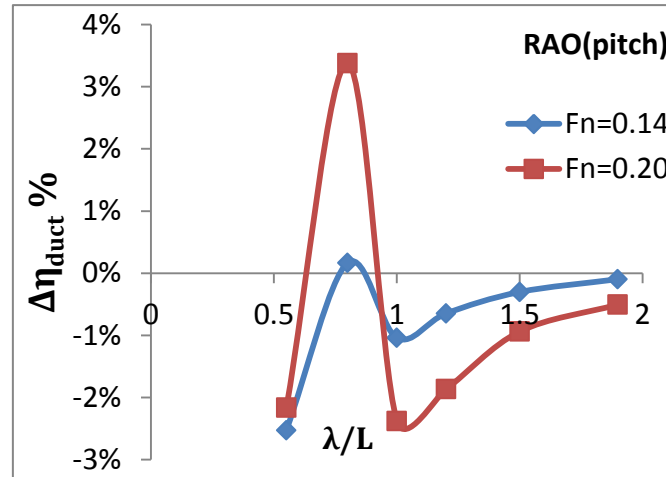


Figure 2-11 The duct's effect on RAO for heave

For heave motion, when  $\lambda/L = 0.55$ , the duct causes slightly more (within 5%) heave motion. The larger velocity promotes more increase in heave. But with wave

becoming longer the duct's effect suddenly changes and instead leads a tiny but most remarkable decrease (within 4%) of heave motion at  $\lambda/L = 0.8$ . For  $\lambda/L \geq 1.5$ , the duct's effect can be neglected.



**Figure 2-12** The duct's effect on RAO for pitch

For pitch motion, when  $F_n = 0.2$ , the duct causes nearly 4% rise around  $\lambda/L = 0.8$ , and beyond narrow range of  $0.7 < \lambda/L < 0.9$ , the duct reduces the motion; while at  $F_n = 0.14$  the duct's effect leads to a decrease under all wave conditions and the effect is most remarkable at  $\lambda/L = 0.55$ .

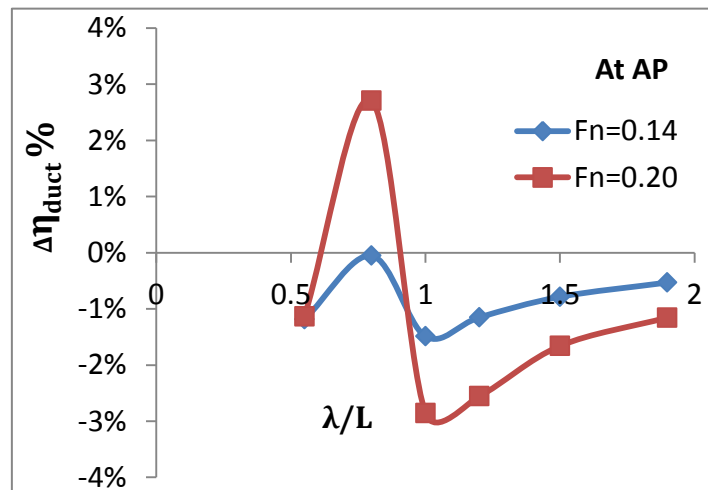


**Figure 2-13** The duct's effect on RAO for vertical acceleration measured at AP

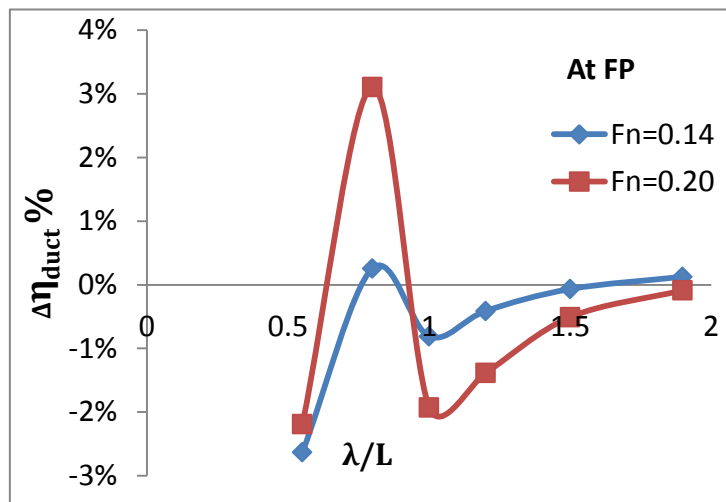


**Figure 2-14** The duct's effect on RAO for vertical acceleration measured at FP

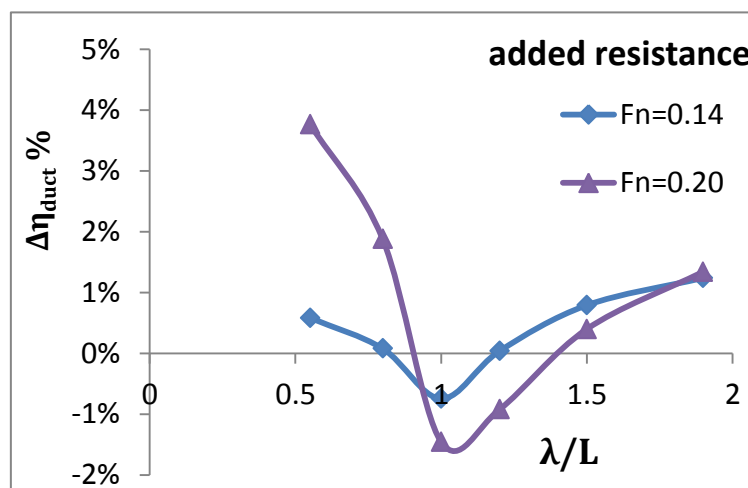


**Figure 2-15** The duct's effect on RAO for added resistance

At smaller velocity, the duct lowers the vertical acceleration at AP a bit for all wave conditions. For higher velocity, the duct shows similarly tendency as its effect on pitch motion. For both velocities, the duct's effect of reducing the acceleration is most remarkable around  $\lambda/L = 1$ .

For acceleration at FP, the duct's effect on acceleration is similar as that on pitch motion for both velocities.

For added resistance, the tendency shows that in narrow range of  $0.8 < \lambda/L < 1.2$  the duct lessens the added resistance in waves, which is most remarkable at  $\lambda/L = 1$ . While beyond this range, when  $\lambda/L < 0.8$ , with increasing wave length, the effect of duct on promoting added resistance becomes less notable; and for longer waves of  $\lambda/L \geq 1.5$ , the duct's effect on added resistance is no longer influenced by waves.

## 2.2.2 Ship speed and powering

The plug-in called Ship Speed & Powering in SHIPX was used to assess speed and power, including resistance and propulsion performance in calm water as well as prediction of speed loss (or added power) in waves. The information for designed open propeller and ducted propeller are shown in *Table 2.3*.

**Table 2.3** Propeller data

Propeller:	Ducted Ka-4.55/19A	Open propeller
Number of propellers:	1	1
Number of blades Z	4	4
Propeller diameter D [mm]	3557.0	4200
Pitch ratio P/D [-]	1.215	0.975
Expanded blade area ratio Ae/Ao [-]	0.697	0.515

Resistance and propulsion performance were first calculated in calm water conditions after initial input of resistance curve and open water characteristics for designed open propeller and ducted propeller. It is noting that for resistance not only two velocities of 13.4 and 9.4[knot] are considered, but also a larger range of velocities from 7 to 16 [knot] are taken into considerations.

Then in regular waves, the total resistance equals to sum of the input calm water resistance and the calculated added resistance in waves from earlier results of SHIPX vessel response. The added resistance values for ducted propeller are calculated from the RAOs for ship with foil, while for the open propeller the RAOs for bare hull are used.

Added resistance can be calculated based on RAO of added resistance in SHIPX vessel response. The default wave amplitude is 1[m] for all different wave periods. The details of added resistance and total resistance at different wave periods for open and ducted propeller are presented in *Appendix B*.

Given wave period, at certain speed, open water diagrams are applied to predict brake power and attainable speed for open and ducted propeller respectively.

Finally the difference of brake power in calm water and in regular waves indicates the added power in waves. Similarly, the reduction of attainable speed in waves refers to speed loss. The data for non-dimensional added power and speed loss are shown *Appendix B*.

The augment of added power is expressed as percentage of power in calm water:

$$\Delta P\% = \frac{P_{wave} - P_{calm}}{P_{calm}} = \frac{\Delta P}{P_{calm}} \quad (2.15)$$



The speed loss is defined as:

$$\Delta V\% = \frac{V_{wave} - V_{calm}}{V_{calm}} = \frac{\Delta V}{V_{calm}} \quad (2.16)$$

The added power and speed loss can be plot as a function of wave conditions in **Figure 2-16**, **Figure 2-17** and **Figure 2-18**. It is expected that added power and seed loss have identical tendency since added power is needed to maintain design speed in order to avoid speed loss.

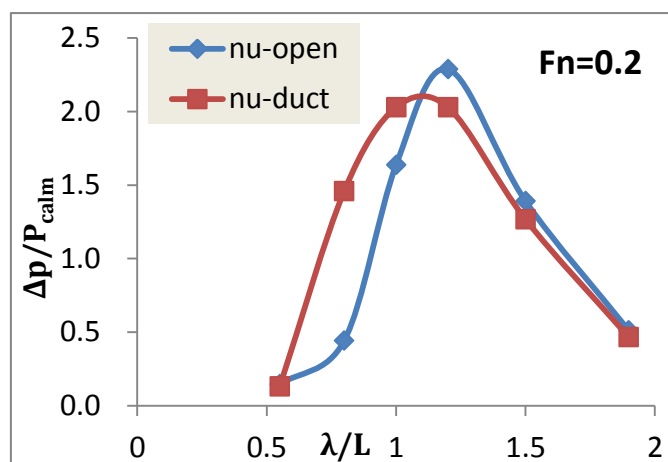


**Figure 2-16** Comparisons of added power for open and ducted propeller at  $F_n=0.2$

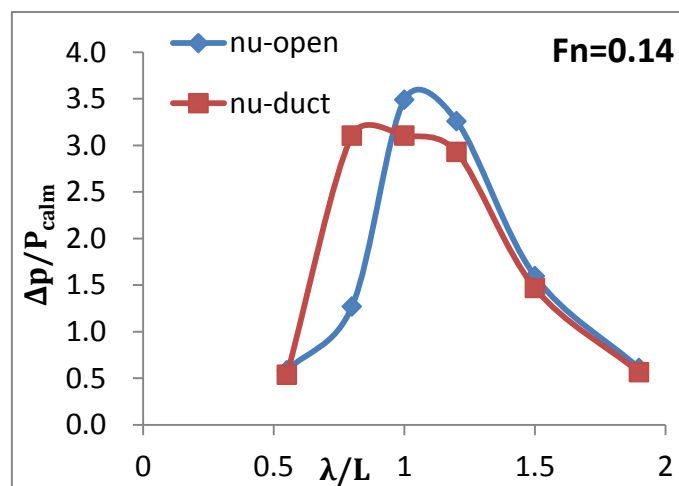


**Figure 2-17** Comparisons of added power for open and ducted propeller at  $F_n=0.14$

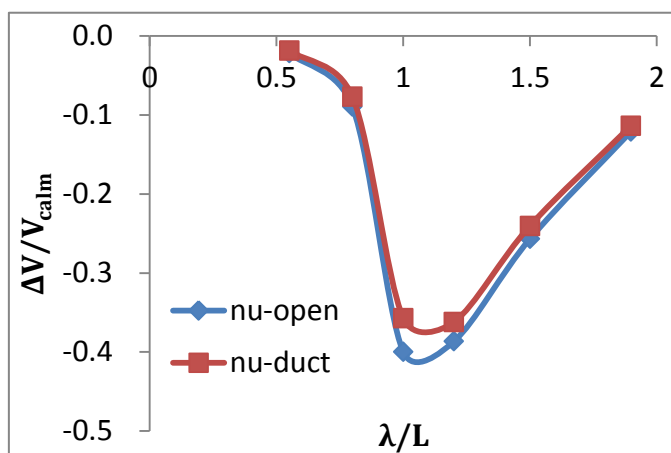


**Figure 2-18** Comparisons of speed loss for open and ducted propeller

And the duct's effect on added power (or speed loss) is shown as **Figure 2-19**.

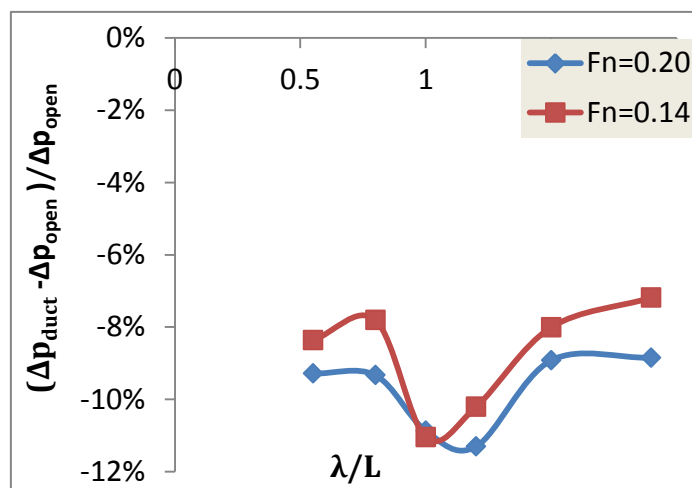


**Figure 2-19** The duct's effect on added power at  $F_n=0.14$  and  $F_n=0.20$

The presence of the duct causes decrease on added power for all wave period. And at smaller forward speed, the duct's effect is more impressive. The duct's effect of reduction on added power shows most remarkable around  $\lambda/L = 1$ .

## 3. Experimental calculation

### 3.1 General information about model tests

A series of experiments were performed in the large towing tank of MARINTEK, with length of 250 [m], depth of 5[m], breadth of 10[m]. Model m3006 Norlines with model scale 22.629 was tested on designed waterline (DWL) 5.5/5.5[m] of full scale.

#### 3.1.1 Model dimensions

The principal dimensions for ship model as well as open propeller and ducted propeller are given in *Table 3.1*, *Table 3.2* and *Table 3.3*.

**Table 3.1** Main dimensions of m3006 under loading conditions

Ship model	symbol	unit	model scale
Length on waterline	$L_{WL}$	[m]	5.267
Length between perpendiculars	$L_{pp}$	[m]	5.197
Breadth at waterline	B	[m]	0.919
Draught at AP/FP	$T_{AP}/T_{FP}$	[m]	0.243
Draught T at $L_{pp}/2$	T	[m]	0.243
Wetted surface	S	[m <sup>2</sup> ]	5.589
block coefficient	$C_B$	[-]	0.657
Displacement	$\nabla$	[m <sup>3</sup> ]	17.249

**Table 3.2** Data for the open propeller used in tests

Open propeller P 1476	Symbol	Unit	model scale
Number of blades	Z	[-]	4
Propeller diameter	D	[mm]	185.60
Pitch ratio at $r/R = 0.7$	$P/D_{0.7}$	[-]	0.975
Blade area ratio	$A_E/A_0$	[-]	0.515

**Table 3.3** Data for the ducted propeller tested in experiments

P1309 with duct 151	Symbol	Unit	model scale
Number of blades	Z	[-]	4
Propeller diameter	D	[mm]	178.30
Pitch ratio at $r/R = 0.7$	$P/D_{0.7}$	[-]	1.297
Blade area ratio	$A_E/A_0$	[-]	0.697

### 3.1.2 Tests set up

The model is connected to the seakeeping carriage with wires in a crow-foot arrangement in the towing tank. The connection is shown in *Figure 3-1* and *Figure 3-2*.

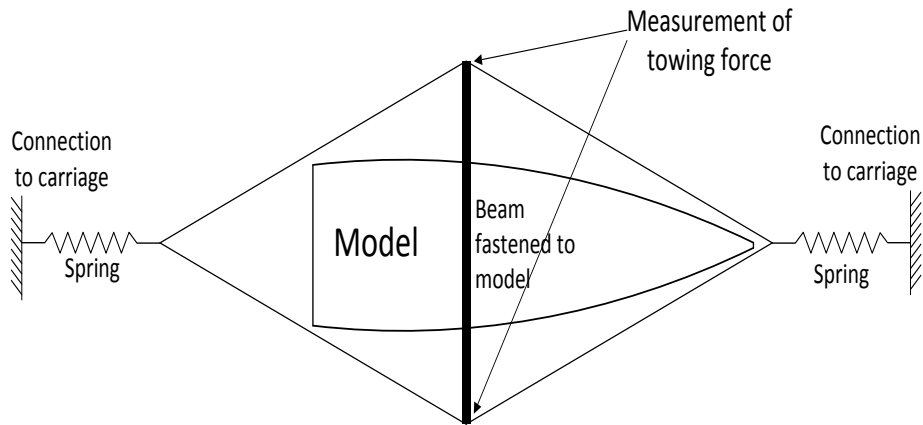


**Figure 3-1** Experimental settings



**Figure 3-2** Model tested in the towing tank

To measure the waves during the tests, two wave probes were installed above the water line in front and behind the carriage (see *Figure 3-3*) respectively to record waves coming from the wave maker and those encountering the model.

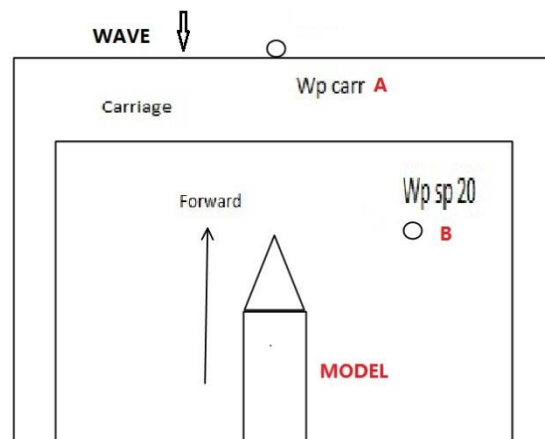


**Figure 3-3** The positions of wave probes

The designed regular wave with different wave amplitude and height conditions are listed as **Table 3.4**.

**Table 3.4** Target waves

$T[s]$	$H[m]$	$\zeta[m]$	$\lambda[m]$	$\lambda/L_{pp}$	$L_{pp}/\lambda$
1.353	0.08	0.04	2.858	0.55	129.92
1.632	0.16	0.08	4.158	0.80	64.96
1.824	0.08	0.04	5.194	1.00	129.92
1.824	0.16	0.08	5.194	1.00	64.96
1.824	0.24	0.12	5.194	1.00	43.31
1.999	0.16	0.08	6.239	1.20	64.96
2.234	0.16	0.08	7.792	1.50	64.96
2.515	0.16	0.08	9.876	1.90	64.96

The model is tested in regular head waves and in calm water, with two velocities corresponding to Froude numbers of  $F_n=0.14$  and  $F_n=0.20$  of which the latter one gives the designed speed.

### 3.1.3 Measurement

The following variables should be measured during the tests:

1. six degree of freedom optical positions of the model
2. vertical acceleration at positions of FP,AP and COG
3. longitudinal acceleration at COG
4. applied tow force
5. incoming and encoutring waves
6. propeller thrust, torqgue and rotatioanl speed
7. duct thrust and vertical force

## 3.2 Wave calibration

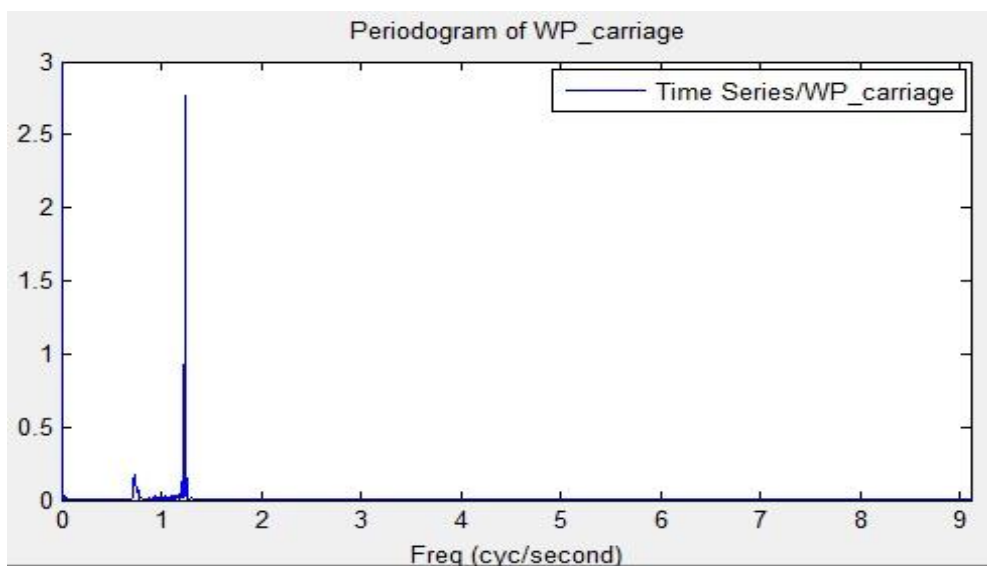
Since the main objectives of this thesis are concerning with waves' influence, it is necessary to maintain the wave homogenous along the towing tank and to avoid instable behavior of waves in space and in time domain, which is the purpose of wave calibration. The results of calibrated waves and comparisons with target waves are shown in the **Table 3.5**.

In addition, it is necessary to ensure that waves travelling from wave maker to the model shows identical characteristic as the calibrated ones. Thus, wave probes installed on the model ship are needed to give information about incoming waves.

**Table 3.5** Calibrated waves compared with target waves

Run no.	$T_D$ [s]	$H_S$ [m]	$T_M$ [s]	$H_M$ [m]	$\frac{T_D}{T_M}$	$\frac{H_D}{H_M}$
8201	1.353	0.08	1.355	$2*\sqrt{2}*0.02905=0.0822$	1.002	1.027
8000	2.186	0.221	2.135	0.2132	0.977	0.965
8210	1.632	0.16	1.629	$2*\sqrt{2}*0.06033=0.1706$	0.998	1.066
8220	1.824	0.08	1.821	$2*\sqrt{2}*0.03035=0.0858$	0.998	1.073
8230	1.824	0.16	1.835	$2*\sqrt{2}*0.05644=0.1596$	1.006	0.998
8240	1.824	0.24	1.869	$2*\sqrt{2}*0.0833=0.2356$	1.025	0.982
8250	1.999	0.16	2	$2*\sqrt{2}*0.05388=0.1524$	1.001	0.952
8260	2.234	0.16	2.242	$2*\sqrt{2}*0.05397=0.1527$	1.004	0.954
8270	2.515	0.16	2.531	$2*\sqrt{2}*0.05674=0.1605$	1.006	1.003

For regular waves only exist one peak frequency because of stable wave period, so by plotting in wave energy spectrum in MATLAB, the peak frequency can be read directly from the **Figure 3-4**.

**Figure 3-4** Energy spectrum of measured waves

As for wave height, standard deviation of wave amplitude is used to calculate average

wave amplitude. See *Figure 3-5*.

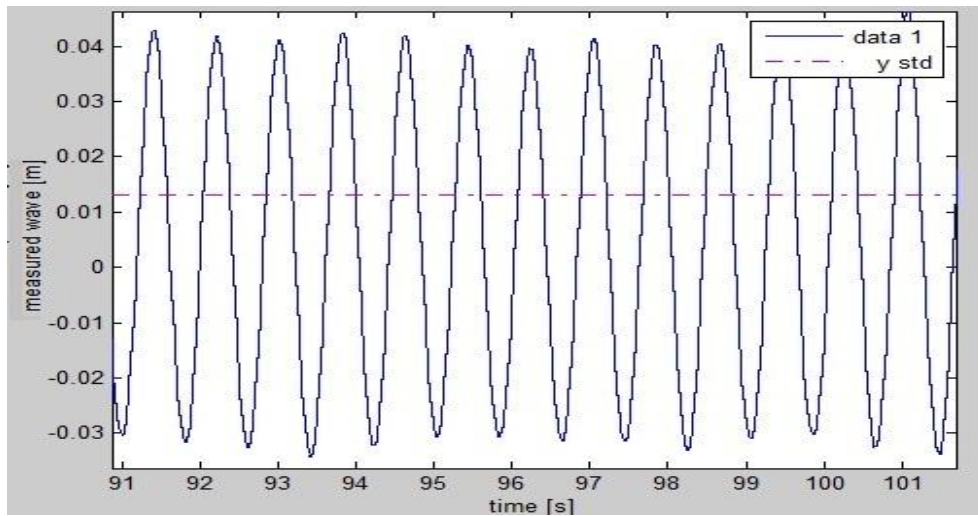


**Figure 3-5** Measured wave during the test by wave probe

The relationship between natural frequency of waves and encounter frequency for head wave is written as:

$$\omega_e = \omega_n + \omega_n^2 V/g \quad (3.1)$$

Where  $\omega_e$  the encounter frequency is directly obtained from figures above;  $\omega_n$  refers to natural frequency of wave;  $V$  is carriage speed and  $g$  is gravity acceleration.

The comparisons of measured waves during the tests by wave probe with calibrated waves when  $F_n = 0.2$  are shown as *Table 3.6*. The difference of encounter frequency and wave height are expressed as

$$\Delta\omega_e \% = (\omega_{e\_measure} - \omega_{e\_calibrated} / \omega_{e\_calibrated}) \times 100\% \quad (3.2)$$

$$\Delta H \% = (H_{measure} - H_{calibrated} / H_{calibrated}) \times 100\% \quad (3.3)$$

**Table 3.6** Comparisons of calibrated waves with measured waves

Wave no.	test.no	$\Delta\omega_e$ %	$\Delta H$ %	Wave no.	test.no	$\Delta\omega_e$ %	$\Delta H$ %
8201	2000	-0.37%	0.00%	8201	2300	-0.54%	-2.27%
8201	2001	-0.39%	1.55%	8210	2310	-1.41%	-6.54%
8210	2010	-1.20%	0.80%	8220	2320	-0.83%	-6.64%
8220	2020	-0.20%	-6.44%	8230	2330	0.62%	1.80%
8220	2021	-0.56%	-4.63%	8240	2040	2.14%	-1.56%
8230	2030	0.61%	2.27%	8250	2050	-0.13%	-1.96%
8230	2031	0.04%	1.72%	8260	2060	0.31%	1.17%
8240	2040	2.23%	1.49%	8270	2070	0.15%	-0.86%

From the tables list above it can be concluded that the calibrated waves are precise to be conduct in tests. And the wave maker produces almost exactly waves needed. It is verified the purpose of wave calibration

### 3.3 Uncertainty and error analysis

Error is the difference between measured value in experiments and true value, while uncertainty is used to indicate the degree of goodness of measurements in experimental results and to estimate a range within which the expected value of error lies [17].

Four repetitions: test 2330, test 2332, test 2333 and test 2334, with open propeller under same regular wave conditions of height 0.16 [m] and period 1.824 [s] were performed to calculate precision errors for 5 variables including rotational speed of propeller, propeller thrust, total thrust of propulsor, torque and applied tow rope force. The recorded data during each four test are shown as **Table 3.7**.

**Table 3.7** Measured results for four repetitions of tests

Test no.	No.	RPS [r/s]	$T_{prop}$ [N]	$T_{total}$ [N]	Q [Nm]	$F_D$ [N]
test2330	1	5.39	-0.76	-0.95	0.02	85.52
	2	8.63	16.27	15.99	0.52	75.58
	3	11.87	45.64	45.33	1.27	49.88
	4	15.73	94.81	94.52	2.47	5.79
test2332	1	5.78	0.55	0.69	0.06	85.35
	2	8.63	16.41	17.06	0.51	76.96
	3	11.87	46.39	47.28	1.28	47.91
test2333	1	5.39	-0.93	-0.69	0.02	88.46
	2	8.63	16.25	16.89	0.51	72.93
	3	11.87	46.18	47.06	1.27	48.48
test2334	1	5.39	-0.89	-0.77	0.02	87.00
	2	8.63	16.29	16.76	0.51	72.96
	3	11.87	45.92	46.77	1.27	46.38

It can be seen that only two different propeller rotational velocities were repeated as marked number 2 and 3 in the table, so for each test of four repetitions precision errors of those five variables were calculated respectively at RPS close to 8.63 and 11.87 [r/s].

A normal distribution is applicable to errors in scientific measurements. The values of density are denoted by  $n(x; \mu, \sigma)$ . The density of the normal random variable  $X$  with



mean  $\mu$  and standard variance  $\sigma$  is defined as

$$n(x; \mu, \sigma) = \frac{1}{\sqrt{2\pi}\sigma} e^{-\frac{1}{2\sigma^2}(x-\mu)^2} \quad (3.4)$$

Where mean value of random variable  $X$  is equal to:

$$\mu = \frac{1}{N} \sum_{j=1}^N X_j \quad (3.5)$$

Standard variance of random variable  $X$  can write as:

$$\sigma = \sqrt{\frac{1}{N-1} \sum_{j=1}^N (X_j - \mu)^2} \quad (3.6)$$

So  $N=4$  for 4 repetitions of tests. It is necessary to give a confidence specification. A 95% confidence estimate is made of measured variable  $X$  so that it would be expected that true value of  $X$  would be in the interval  $(\mu \pm X)$  about 95 times out of 100 [17].

A normal distribution can be transferred into a standard normal distribution  $n(z; 0,1)$

by defining  $Z = \frac{X-\mu}{\sigma}$ , where  $Z$  is seen to be a standard normal variable, with mean 0 and variance 1.

The confidence interval is written as

$$\text{Prob}(-t_0 < Z < t_0) = \gamma \quad (3.7)$$

With  $\gamma$  is the confidence interval, given  $\gamma = 0.95, t_0 \approx 1.96$ .

Hence the precision limit for one sample  $P_X$  and that for average of  $N$  samples can be found  $P_{\bar{X}}$  as **Table 3.8** and **Table 3.9** shown.

$$P_X = t_0 \sigma \quad (3.8)$$

$$P_{\bar{X}} = t_0 \sigma / \sqrt{N} \quad (3.9)$$

**Table 3.8** Precision limit for one sample at 95% confidence estimate

$P_X$	RPS [Hz]	$T_{prop}$ [N]	$T_{total}$ [N]	Q [Nm]	$F_D$ [N]
No.2	0.00173	0.124	0.803	0.00641	3.39
No.3	0.000974	0.555	1.49	0.00685	2.46

**Table 3.9** Precision limit for 4 samples at 95% confidence estimate

$P_{\bar{X}}$	RPS[Hz]	$T_{prop}$ [N]	$T_{total}$ [N]	Q [Nm]	$F_D$ [N]
No.2	0.000867	0.0623	0.401	0.00320	1.70
No.3	0.000487	0.278	0.747	0.00342	1.23

Then precision errors for one sample and for 4 samples are defined respectively as

$$E_x = \mu / P_X \quad (3.10)$$

$$E_{\bar{x}} = \mu / P_{\bar{X}} \quad (3.11)$$

The precision errors for 5 selected variables can be found as **Table 3.10**.

**Table 3.10** Precision error

$\mu/P_X$	RPS [Hz]	$T_{prop}$ [N]	$T_{total}$ [N]	Q[Nm]	$F_D$ [N]
No.2	0.020%	0.764%	4.818%	1.251%	4.548%
No.3	0.008%	1.206%	3.204%	0.539%	5.116%
$\mu/P_{\bar{X}}$	RPS [Hz]	$T_{prop}$ [N]	$T_{total}$ [N]	Q[Nm]	$F_D$ [N]
No.2	0.010%	0.382%	2.409%	0.625%	2.274%
No.3	0.004%	0.603%	1.602%	0.269%	2.558%

The results indicate that precision errors can be reduced by repetitions of tests. Additionally it can be seen that the measurement of tow rope force gives largest precision errors.

### 3.4 The effect of duct on motions and accelerations

The motion variables taken into consideration are heave, pitch and accelerations in Z direction at FP and AP positions. In order to see the effect of duct on motions and accelerations under different wave conditions, non-dimensional experimental data are drawn into figures.

The definition of RAO is expressed as the ratio of standard deviation of motions or accelerations over standard deviation of calibrated wave as shown:

$$\sigma_{\eta} / \sigma_w = RAO(\eta) \quad (3.12)$$

where  $\eta$  represents motion variables, including heave, pitch, and vertical accelerations.

The deviation caused by presence of the duct on motion, added resistance and added power between the results of open propeller and ducted propeller is calculated as:

$$\Delta\eta_{duct} \% = \frac{\eta_{duct} - \eta_{open}}{\eta_{open}} \times 100\% \quad (3.13)$$

Here  $\eta$  represents the ship motion variables, added resistance and added power.

#### 3.4.1 RAO for heave motion

The results of RAO for heave motion at two velocities for open propeller and ducted propeller are shown into **Figure 3-6**. And the difference due to presence of duct on RAO for heave motion is plot into **Figure 3-7**.

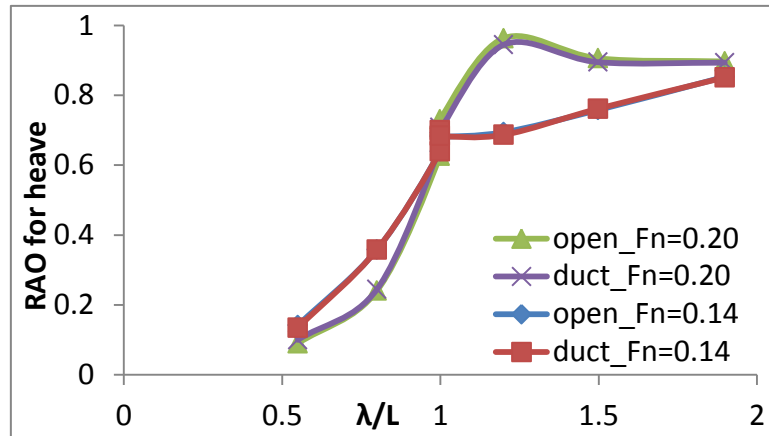


**Figure 3-6** Comparisons of RAO for heave motion at  $F_n = 0.14$  and  $F_n = 0.2$

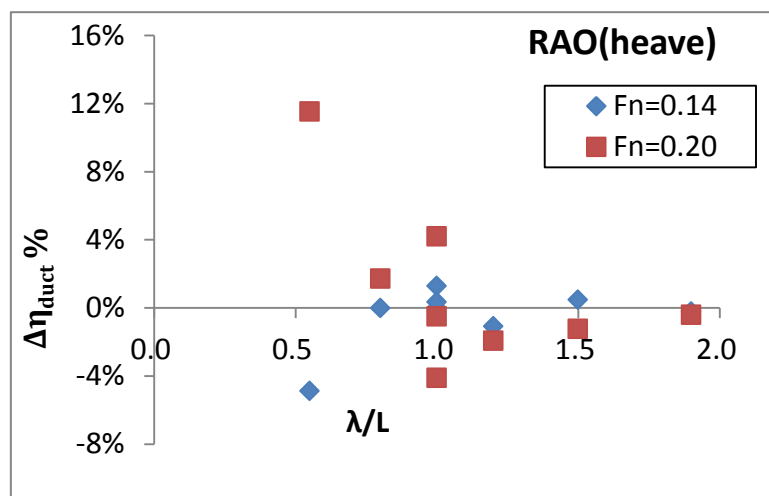


**Figure 3-7** The duct's effect on heave motion

The duct's effect on heave motion is of speed dependence.

When  $F_n = 0.14$ , the duct generally causes a tiny decrease on heave motion, except around  $\lambda/L = 1.0$ . When  $F_n = 0.20$ , the presence of the duct will increase heave motion by 11.54% at  $\lambda/L = 0.55$ . But this effect of promoting heave motion fades away near  $\lambda/L = 1.0$ . The deviation of RAO for heave between open propeller and ducted propeller is narrowly within  $\pm 2.0\%$  when  $\lambda/L$  becomes bigger than 1.2.

The peak of RAO for heave motion lays on different  $\lambda/L$  values for two velocities because of change of encounter frequencies. The peak moves up and right in the **Figure 3-6** with larger  $\lambda/L$  values at higher speed.

In sum, duct has small influence on heave motion. This may be due to the weight of duct is so small compared with ship's weight, so as a whole total mass doesn't change too much, vertical damping effect will not much influenced by existence of duct.

### 3.4.2 RAO for pitch motion

RAO for pitch motion are dependent of forward speed. Unlike heave motion, added mass and damping terms of pitch motion are functions of forward speed [18]. But the dependence of pitch motion on speed is less notable compared with heave motion in the range of  $0.8 < \lambda/L < 1.5$ .

Also the encounter frequency in head wave will increase with forward speed. The duct lowers the pitch motion for all wave periods at  $F_n = 0.20$ , although this effect is very small (within 4%). While for smaller velocity of  $F_n = 0.14$ , the duct leads to remarkable rise of pitch motion at  $\lambda/L = 0.55$ , with longer waves this effect suddenly changes and tends to reduce pitch motion.

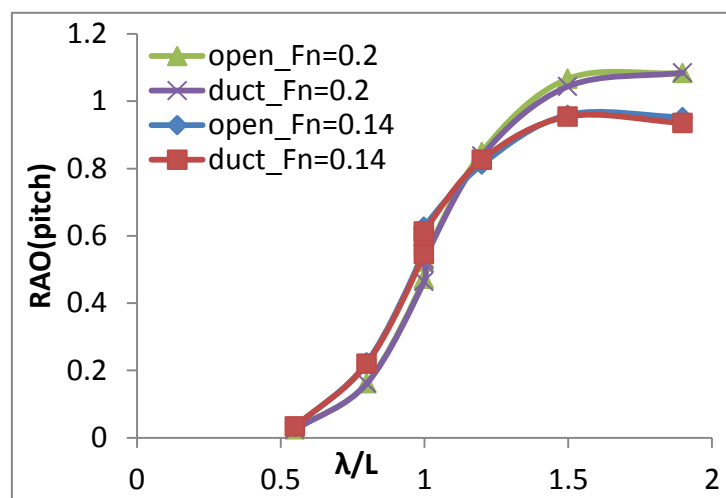


**Figure 3-8** Comparisons of RAO for pitch motion at  $F_n = 0.14$  and  $F_n = 0.2$

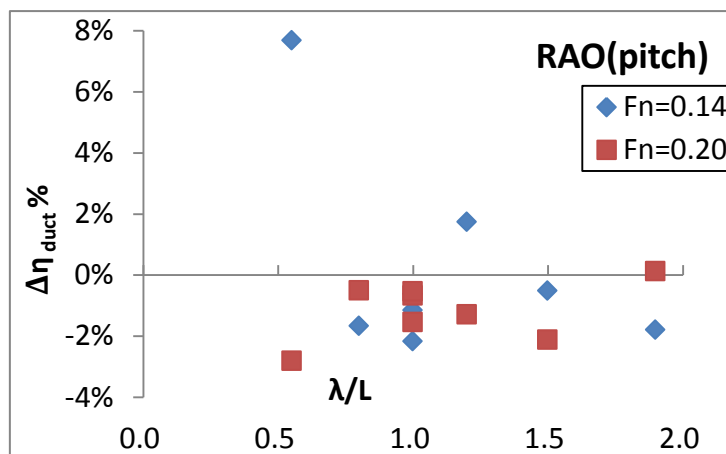


**Figure 3-9** The duct's effect on pitch motion

As conclusion, the duct's influence on reducing pitch motion is small, but this effect is speed dependent and generally increases with  $\lambda/L$ .

### 3.4.3 RAO for acceleration in Z-direction

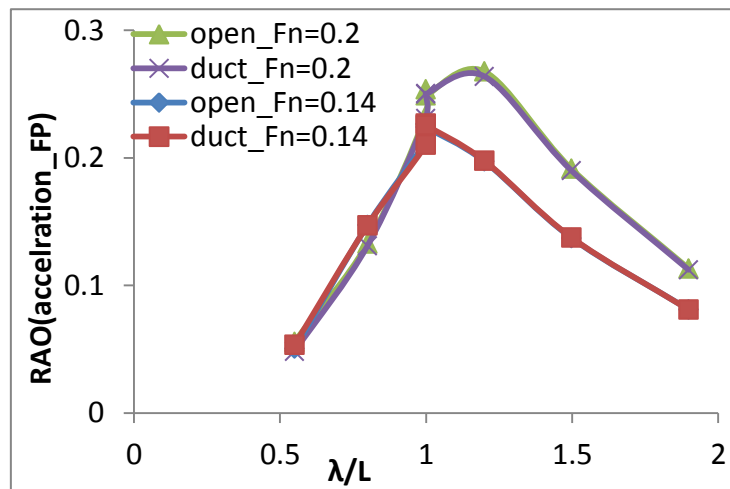


Figure 3-10 Comparisons of RAO for acceleration measure at FP

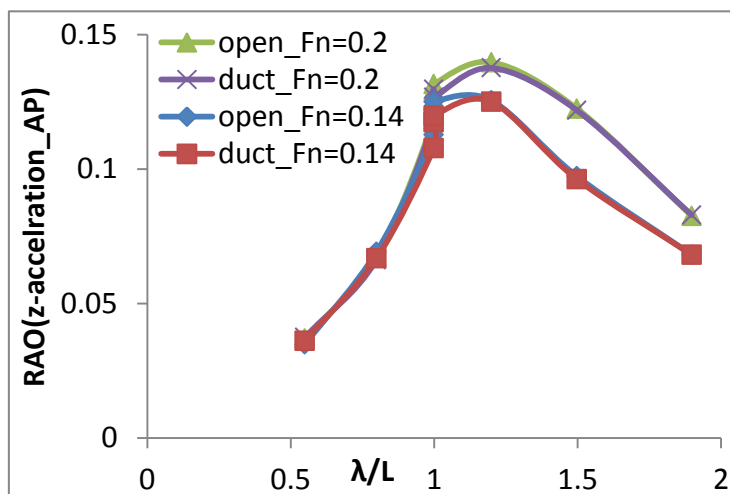


Figure 3-11 Comparisons of RAO for acceleration measure at AP

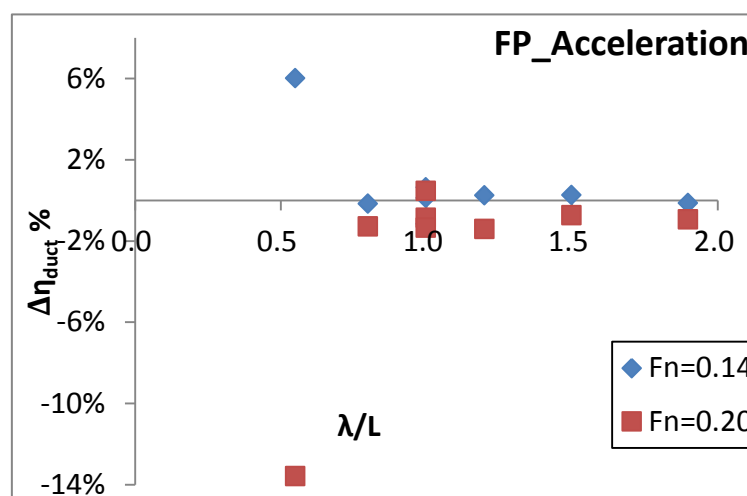
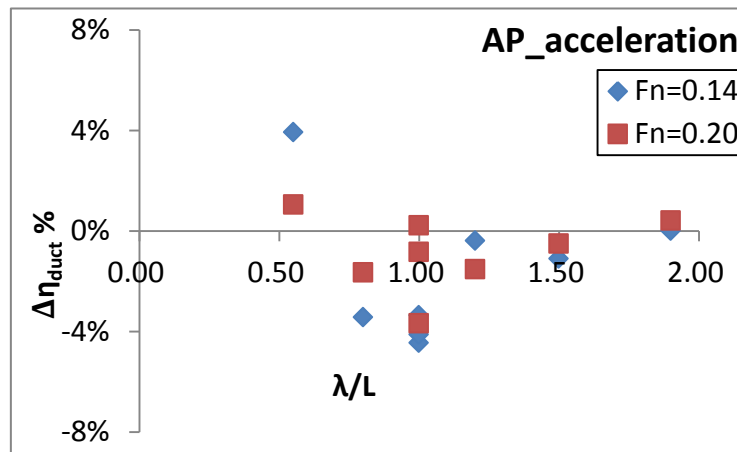


Figure 3-12 The duct's effect on vertical acceleration measured at FP



**Figure 3-13** The duct's effect on acceleration measured at AP.

Measured at FP, the duct leads to most impressive influence on vertical acceleration at shortest wave of  $\lambda/L=0.55$ , for both velocities. And the duct's influence on acceleration is function of speed for  $\lambda/L < 1$ . While for acceleration measured at AP, the duct's effect shows more dependence on wave period rather speed.

This may be result of the fact that interaction between a ducted propeller and stern is more influenced by waves conditions while for same shape of bow the interactions between bow and the waves are very connected with forward speed.

As conclusions, the duct's effect is function of measured position, wave period and forward speed.

### 3.5 The duct's effect on added resistance

During the experiments, force gauges were stick on the model to measure the tow rope force and propeller or total thrust. The model was first tested in calm water, and then in regular waves. Therefore the added resistance for each wave condition is the deviation of resistance in calm water and in regular wave.

Same loading conditions are considered to calculate propulsive factors for model tests. Tow rope force is applied as correction for frictional difference, correlation allowance, and scale effects so that model propeller can be running under same propeller loading as full scale ship propeller [11]. During the experiments British method was adopted and the model is connected to the carriage through a force transducer that measures the resistance force.

Based on the linear relationship (see *Equation 3.14*) between tow rope force and thrust, resistance of model was obtained by finding the intersection of the line with y-axis.

$$(1 - t)T + F_D = R_{TM} \quad (3.14)$$

where  $T$  refers to propeller thrust for open propeller and total thrust for ducted

propeller.

Take an example of test 2001 with ducted propeller. The linear relationship between the total thrust and tow rope force gives the resistance as shown as *Figure 3-14*.

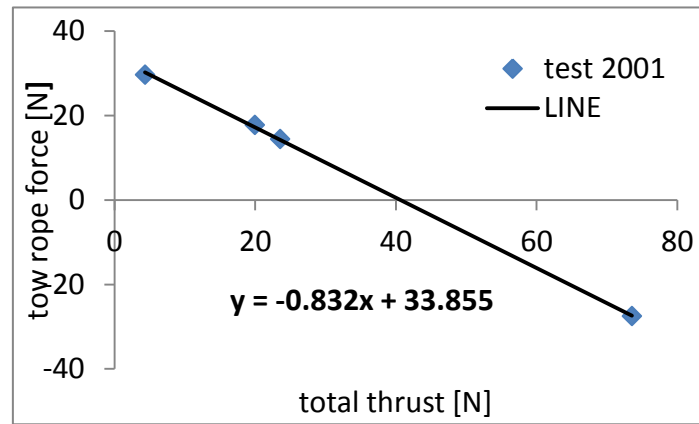


**Figure 3-14** Linear relationship between thrust and tow rope force for test 2001

So the resistance for test 2001 is 33.86 [N]. This method is applied to all tests to get resistance under different wave conditions. Added resistance  $R_{AW}$  results from the difference of calculated resistance in waves and in calm water. The non-dimensional experimental data are presented as *Table 3.11*.

**Table 3.11** Added resistance varying with wave conditions at  $F_n = 0.14$

$\frac{R_{AW}}{\rho g \zeta^2 B^2 / L}$	$F_n = 0.14$	Ducted propeller			Open propeller		
		test	Raw	non	test	Raw	non-di
Wave no.	$\lambda / L$						
8201	0.55	2100	6.68	2.48	2200	4.89	1.82
8210	0.80	2110	36.47	3.14	2210	34.80	3.00
8220	1.00	2120	14.71	5.01	2220	14.00	4.77
8230	1.00	2130	52.05	5.13	2230	51.90	5.11
8240	1.00	2140	102.93	4.65	2240	105.81	4.78
8250	1.20	2150	32.87	3.55	2250	32.81	3.54
8260	1.50	2160	14.81	1.59	2260	14.37	1.55
8270	1.90	2170	5.19	0.51	2270	4.59	0.45

**Table 3.12** Added resistance varying with wave conditions at  $F_n = 0.20$ 

$\frac{R_{AW}}{\rho g \zeta^2 B^2 / L}$	$F_n = 0.20$	Ducted propeller			Open propeller		
Wave no.	$\lambda / L$	test	Raw	non	test	Raw	non-di
8201	0.55	2001	7.65	2.84	2300	6.79	2.52
8210	0.80	2011	33.51	2.89	2310	35.43	3.05
8220	1.00	2020	19.21	6.54	2320	18.76	6.39
8230	1.00	2031	59.73	5.88	2330	61.15	6.02
8240	1.00	2040	119.91	5.42	2340	123.05	5.56
8250	1.20	2050	52.91	5.71	2350	54.89	5.93
8260	1.50	2060	27.58	2.97	2360	27.74	2.99
8270	1.90	2070	11.47	1.12	2370	11.01	1.07

**Table 3.13** The duct's effect on added resistance

$\Delta \left( \frac{R_{AW}}{\rho g \zeta^2 B^2 / L} \right) \%$	$\lambda / L$	$F_n = 0.14$	$F_n = 0.20$
8201	0.55	36.72%	12.58%
8210	0.80	4.79%	-5.42%
8220	1.00	5.08%	2.36%
8230	1.00	0.29%	-2.33%
8240	1.00	-2.72%	-2.55%
8250	1.20	0.20%	-3.62%
8260	1.50	3.07%	-0.57%
8270	1.90	13.06%	4.17%

To visualize the duct's influence on added resistance in waves, results are shown into figures as follows:



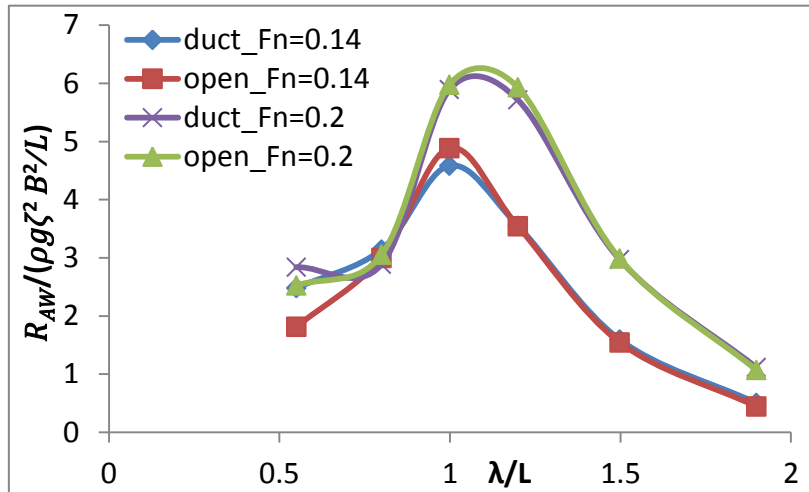


**Figure 3-15** Comparisons of added resistance for open and ducted propeller

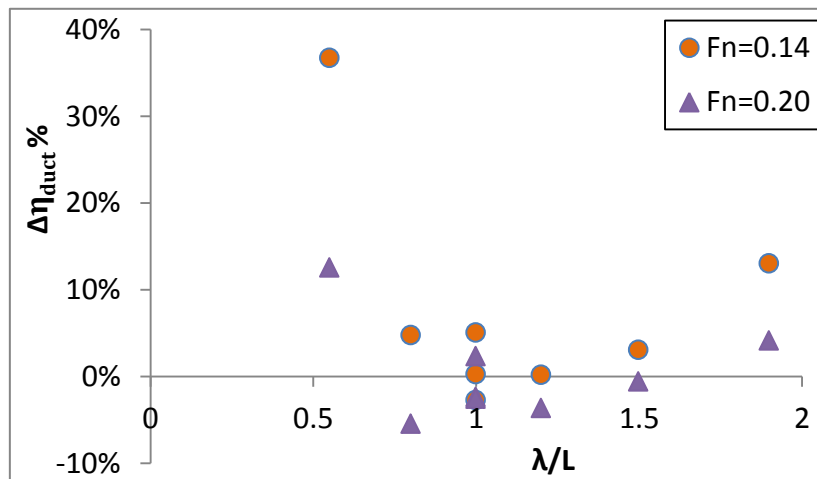


**Figure 3-16** The duct's effect on added resistance

The presence of duct generally introduces more added resistance compared with open propeller at same wave condition for two carriage velocities. However, this effect changes in waves and depends on forward speed.

At  $F_n = 0.14$ , with  $\lambda/L = 0.55$ , duct makes contribution of increasing striking 36.7% added resistance; when wave becomes longer till  $\lambda/L = 1.0$  duct's effect lowers to 5% increase of added resistance. When  $\lambda/L < 1.0$ , the duct's effect on added resistance becomes smaller with increasing wave length. This is due to the fact that the contribution of wave reflection to added resistance decreases with longer waves, ship motion becomes more important to added resistance [19].

When  $\lambda/L \geq 1.0$ , the duct's effect extends with longer waves. This may be explained by the fact that for longer waves when the radiation wave dominates, the existence of duct changes the wave pressure field after the stern, and thus the interaction of ducted propeller and stern leads to more added resistance.

## 3.6 Analysis of propulsive factors change due to waves

### 3.6.1 Basic definition

The behind-hull characteristics of the propeller system are very important to gain overview of the prediction of ship propulsion. The basic definitions for certain propulsive factors of interest are list below.

#### 1. Mean Taylor wake fraction

To represent the wake field, Taylor's method with the ratio of tangential and radial velocities is used to define the wake fraction  $w$ .

$$w = 1 - \frac{v_a}{V_s} \quad (3.15)$$

$V_s$  is the ship speed, and  $v_a$  is mean speed of advance.

#### 2. Thrust deduction factor

The variation in pressure field along the hull due to existence of propulsor leads to decrease in propeller effective thrust, to express the reduction of thrust, thrust deduction factor is introduced as  $t$ .

$$R = T(1 - t) \quad (3.16)$$

$R$  is resistance of the ship, and  $T$  is representative of thrust, which is propeller thrust for open propeller and total thrust for ducted propeller.

#### 3. Relative rotative efficiency

To consider the difference of torque characteristic of the propulsor in open water and after-stern wake field, relative rotative efficiency is defined as:

$$\eta_R = \frac{K_{Q0}}{K_Q} \quad (3.17)$$

where  $K_{Q0}$  is the torque efficiency measured under open water conditions at identical advance ratio [1].

### 3.6.2 Interpolation method

For each test, force variables including thrust, torque, and tow rope force were recorded corresponding to three or four different rotational speed of propeller. In order to find relevant values at self-propulsion point, interpolation method is applied and the details of the process are described as following:

1).Tow rope force at self-propulsion point for certain carriage speed is calculated. Details of calculation of tow rope force can be checked in Appendix C.

The tow rope forces are list in **Table 3.14**.

2).At propulsive point, corresponding RPS was interpolated from the relationship between experimental results of RPS and tow rope force, which is in principal a

straight line. Take an example of the interpolation for test 2200. By input of tow rope force 9.145 [N], it reads off corresponding RPS from the linear expression. See *Figure 3-17*.

3). Then thrust and torque at self-propulsion point would be similarly interpolated from 1<sup>st</sup> order polynomial curves by providing interpolated RPS from step 2. See *Figure 3-18* and *Figure 3-19*.

**Table 3.14** Tow rope force at self-propulsion point for two velocities

$F_n$	$V_S$ [knot]	$V_M$ [m/s]	$F_D$ [N]
0.14	9.4	1.016	5.190
0.20	13.4	1.449	9.145

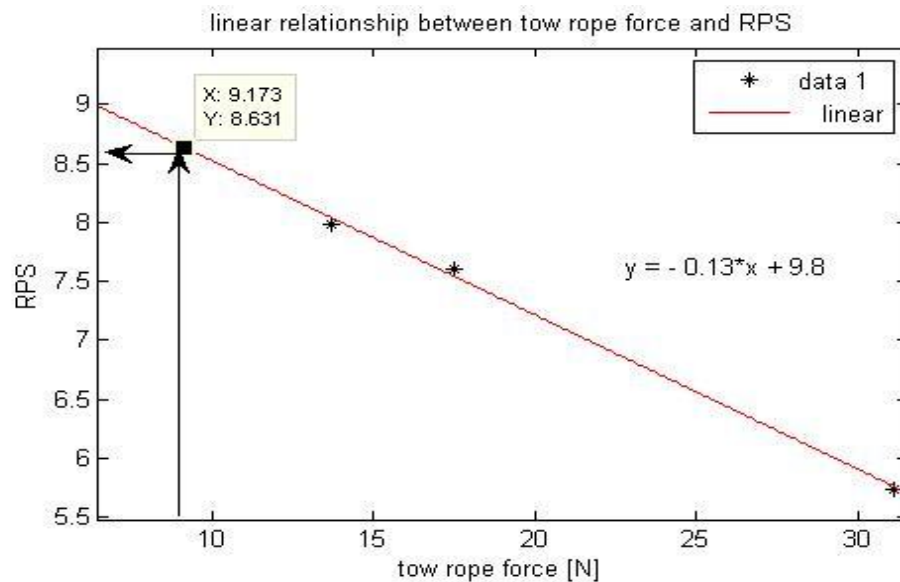


**Figure 3-17** Read out RPS given tow rope force at self-propulsion point

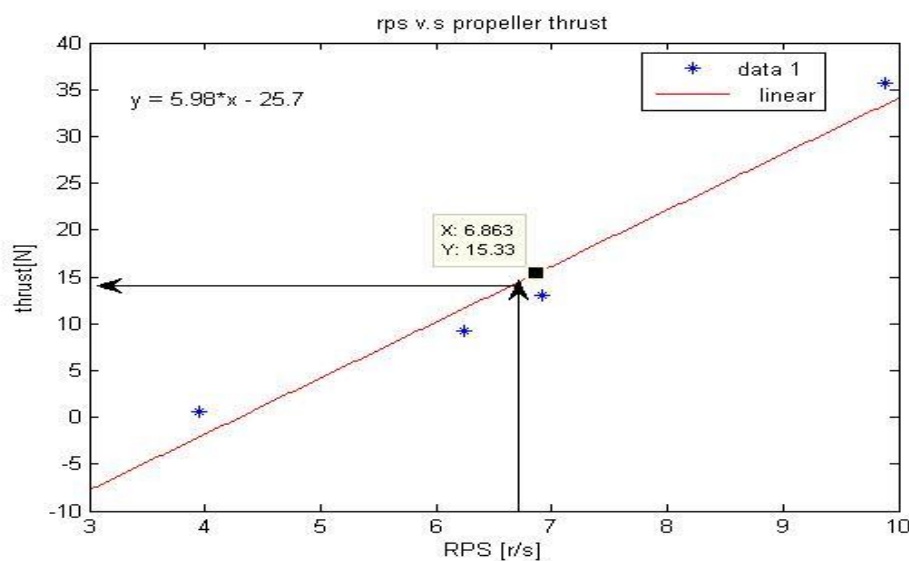


**Figure 3-18** Read out thrust given interpolated RPS at self-propulsion point

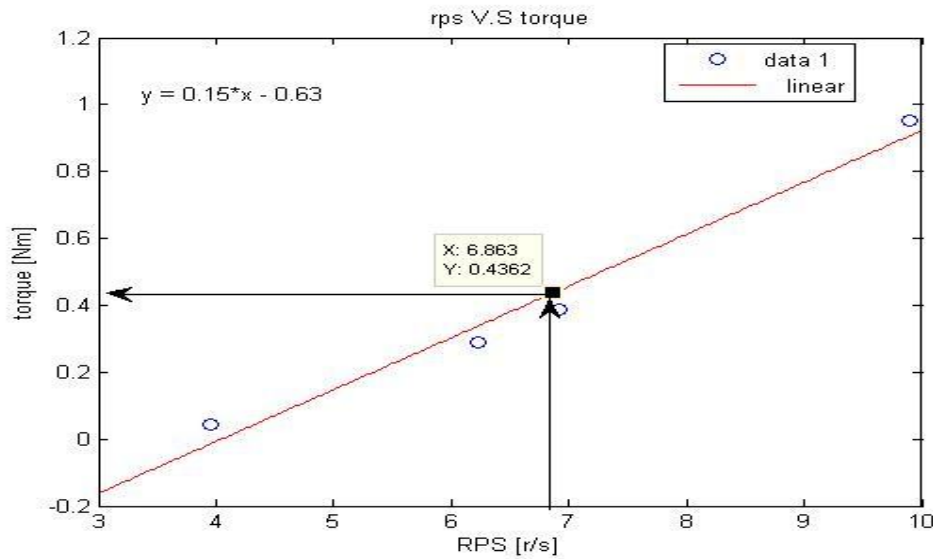


**Figure 3-19** Read out torque given interpolated RPS at self-propulsion point

### 3.6.3 Calculation of propulsive factors

The process of making analysis of propulsion tests to obtain propulsive factors is shown as following [1]:

1. Based on the relationship for thrust and tow force, thrust deduction is expressed as:

$$t = 1 - \frac{R_{TM} - F_D}{T} \quad (3.18)$$

where  $T$  refers to interpolated thrust given tow rope force and  $R_{TM}$  is the resistance of the test.

2. Determine the thrust coefficient, which is defined as

$$K_T = \frac{T}{\rho n^2 D^4} \quad (3.19)$$

where  $n$  is interpolated RPS for calculated tow rope force and  $D$  is diameter of the propeller.

3. Find torque coefficient:

$$K_Q = \frac{Q}{\rho n^2 D^5} \quad (3.20)$$

where  $Q$  is interpolated torque.

4. Calculate advance coefficient:

$$J = \frac{V}{nD} \quad (3.21)$$

5. Using thrust identity, which means  $K_{T0} = K_T$ , by input of calculated thrust coefficient  $K_T$ , advance ratio in open water  $J_0$  is obtained from open water diagram.

The open water properties of  $K_{Q0}$ ,  $\eta_0$  corresponding to  $J_0$  are determined, so wake fraction is computed as:

$$w = 1 - \frac{J}{J_0} \quad (3.22)$$

5. Relative rotative efficiency is written as:

$$\eta_R = \frac{K_{Q0}}{K_Q} \quad (3.23)$$

6. Hull efficiency is defined as:

$$\eta_H = \frac{1-t}{1-w} \quad (3.24)$$

7. Quasi-propulsive coefficient is computed by:

$$\eta_D = \eta_0 \eta_H \eta_R \quad (3.25)$$

Details of results can be checked in Appendix D.

In order to show the influence of waves on those propulsive factors results of calm water are set as reference in the same figures.

In the following figures from **Figure 3-20** to **Figure 3-27**, the values of propulsive factors in calm water are presented by horizontal lines and 'hr' represents relative rotative efficiency  $\eta_R$ .

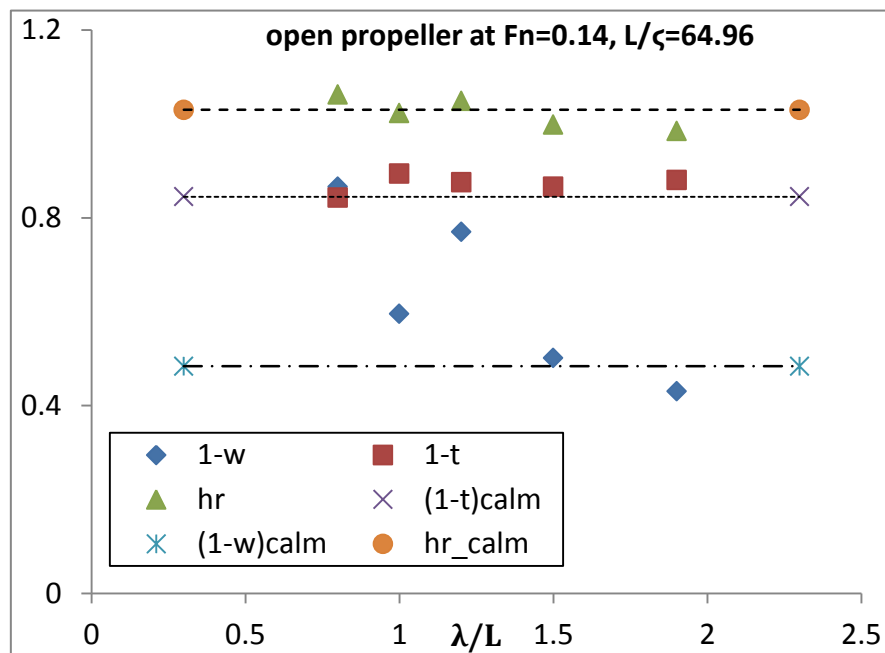


**Figure 3-20** The effect of wave length on propulsive factors for open propeller at  $F_n = 0.14$

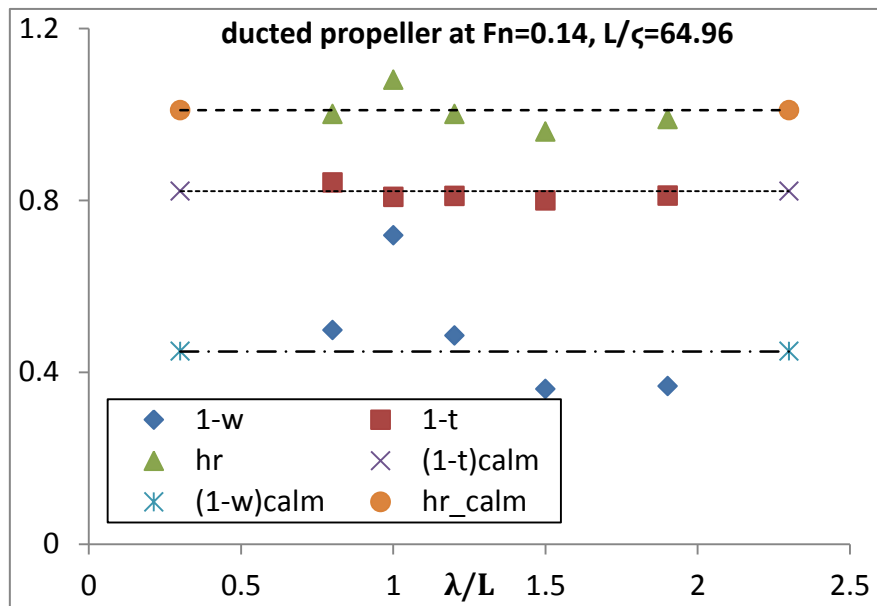


**Figure 3-21** The effect of wave length on propulsive factors for ducted propeller at  $F_n = 0.14$

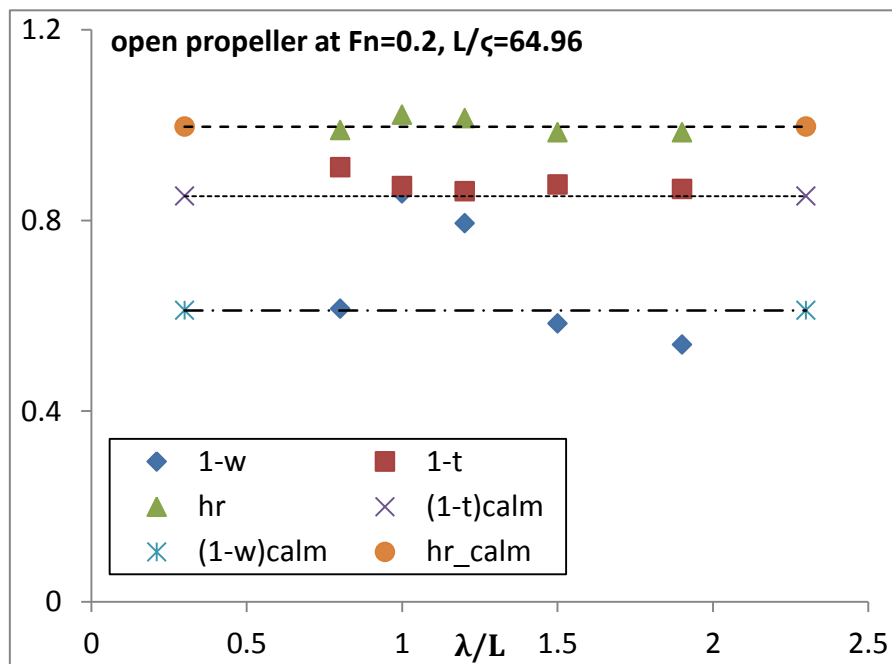


**Figure 3-22** The effect of wave length on propulsive factors for open propeller at  $F_n = 0.2$

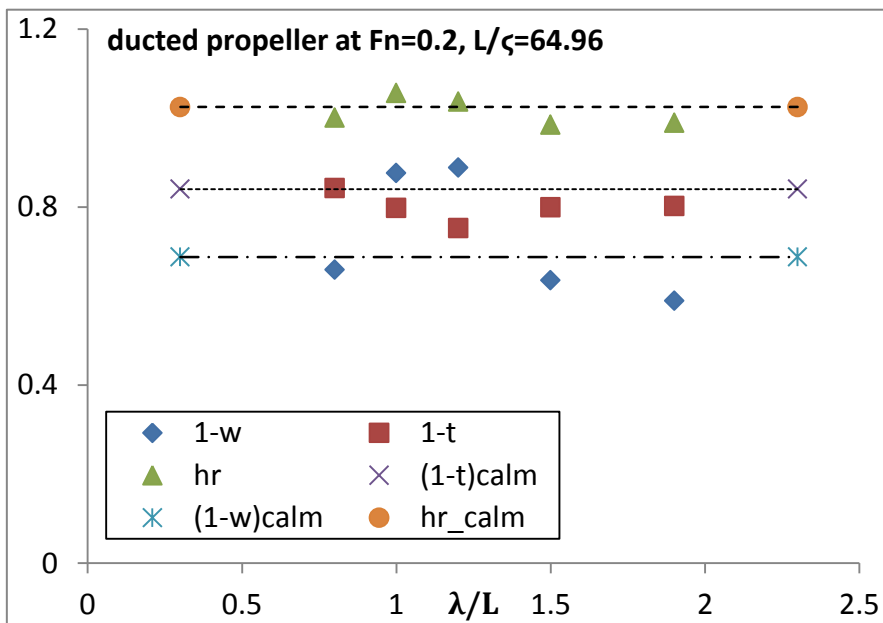


**Figure 3-23** The effect of wave length on propulsive factors for ducted propeller at  $F_n = 0.2$

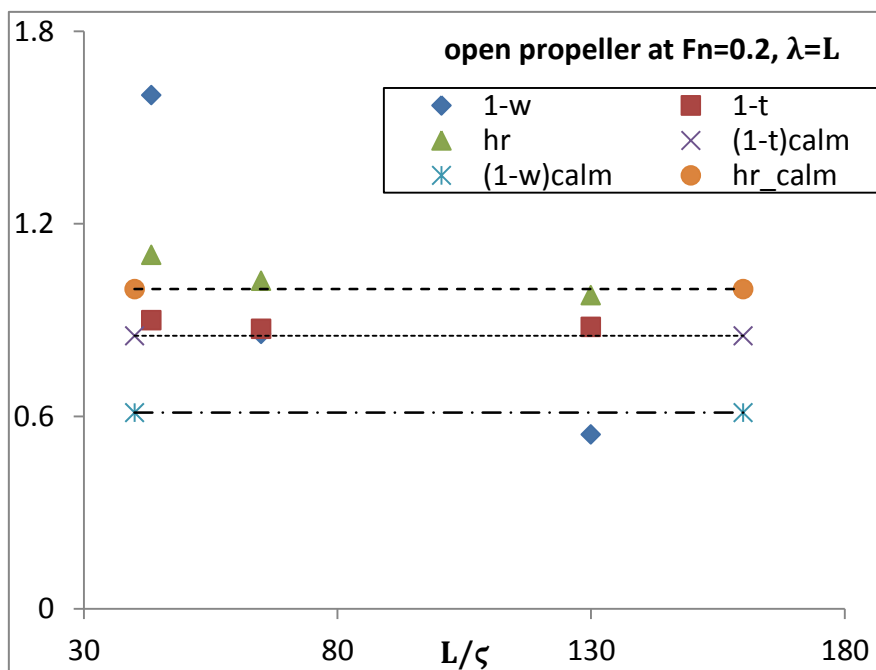


**Figure 3-24** The effect of wave height on propulsive factors for open propeller at  $F_n = 0.2$

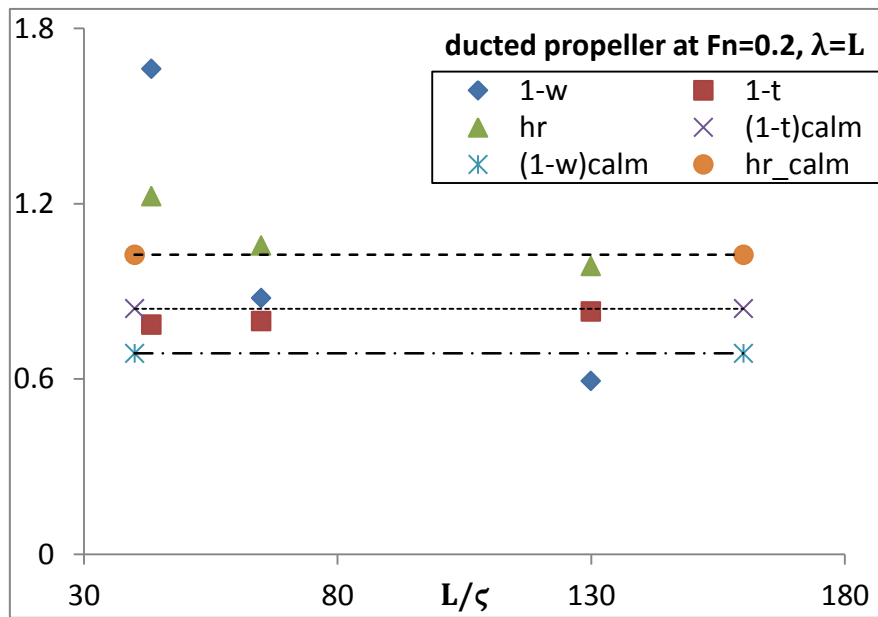


**Figure 3-25** The effect of wave height on propulsive factors for ducted propeller at  $F_n = 0.2$

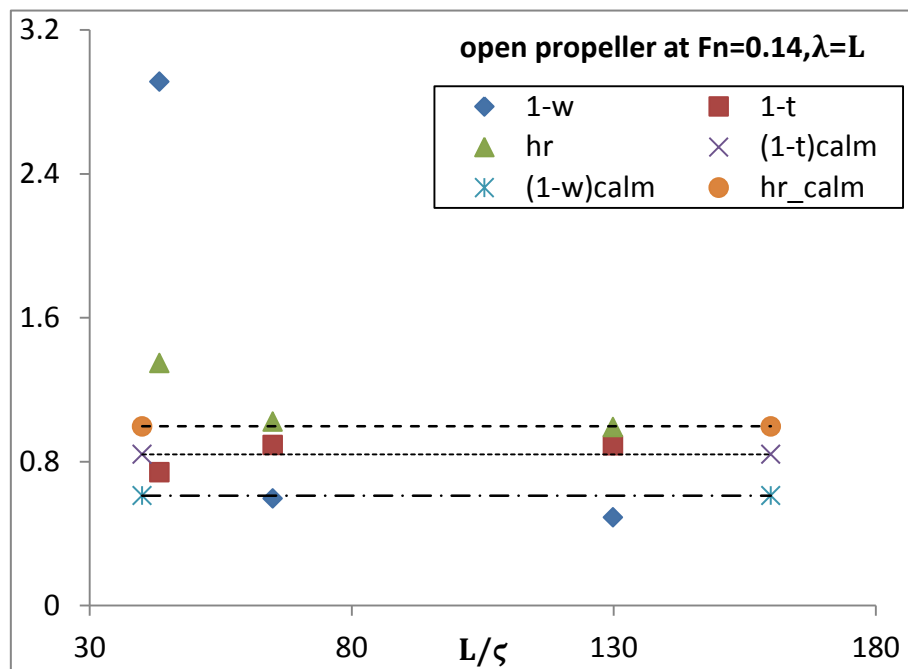


**Figure 3-26** The effect of wave height on propulsive factors for open propeller at  $F_n = 0.14$



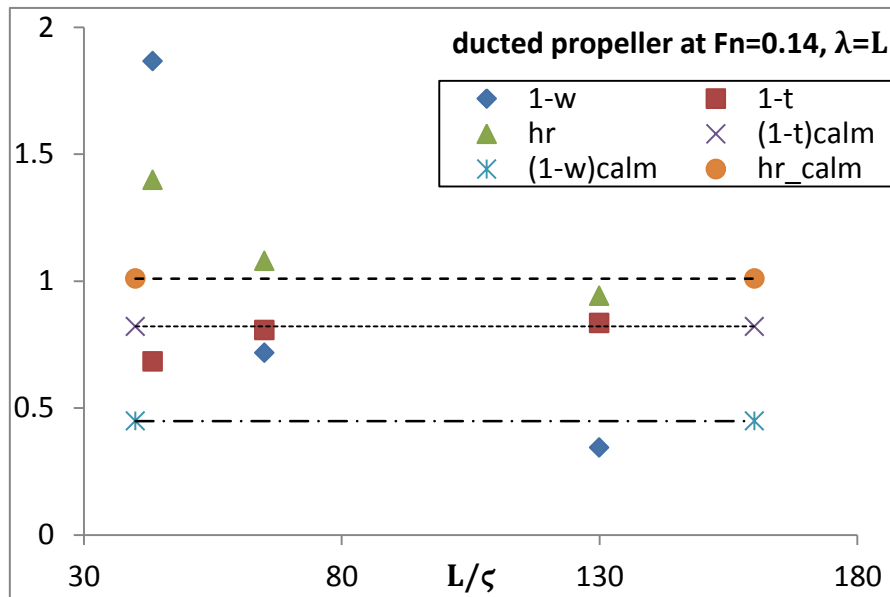


**Figure 3-27** The effect of wave height on propulsive factors for ducted propeller at  $F_n = 0.14$

### 3.6.4 Observations from results and figures

For each test, analyze the recorded data to find propulsion factors. Compared with calm water performance, the results of interpolated method show large uncertainty, for example, wake becomes negative for server conditions. The reasons for chaotic results obtained from interpolation methods are as follows:

First as it was shown in uncertainty analysis, measured tow rope force gives the highest uncertainty during the tests, which means the method based on measured tow rope force naturally contains high uncertainty.

What's more, to reduce data scatter, only first-order of polynomial is applied, and interpolated data may be outside the range of those recorded data of RPS, which leads to the wake becomes negative under much too high propeller rotational speed that would cause cavitation and ventilation theoretically. For test 2210, 2230,2240,2250 with open propeller, and 2130, 2140 with ducted propeller at carriage speed of 1.016[m/s]; as well as test 2332,2333,2334,2340 with open propeller, and test2030,2040,2050 with ducted propeller at 1.449[m/s], their interpolated RPS for given tow rope force are higher than biggest testing RPS. So their propulsive factors are questionable to be directly compared with the results of the rest tests. And this may be reason for sudden up and down of points in the figures.

For this situation where interpolated RPS is outside the range of recorded RPS, extrapolation is required but it is of large uncertainty, so the biggest measured RPS during one test is used for calculation for instead. This may certainly introduce other

uncertainty in results of propulsive factors, for instance, to change the self- propulsion points. The details of the results are shown in Appendix D.

As it can be seen from **Figure 3-20** to **Figure 3-27**, the following observations can be made:

1. The thrust deduction arrives at a minimum around  $\lambda/L=0.55$ , which is close to natural period of pitch motion. And this is clarified in Faltinsen and Minsaas [5]. The presence of duct leads to a rise in thrust deduction and this effect is larger in waves than in calm water. At  $L/\zeta=64.96$ , duct's effect narrows with longer waves. The exception takes place at  $\lambda/L = 0.8$  and  $F_n=0.14$ , where duct reduces the thrust deduction. This may due to the error of changing propulsion point made by using maximum RPS from the tests rather than interpolation of tests results. At  $\lambda/L = 1$  and  $F_n=0.2$ , duct's effect enlarges with higher waves. The tendency is not clear for  $F_n=0.14$  and this may be the same error of changing the propulsion points at  $L/\zeta=64.96$  and  $L/\zeta=43.3$ .
2. The variation of wake fraction due to duct's presence is speed-dependence under same wave conditions. At  $F_n=0.14$ , the duct promotes the wake fraction both in regular waves and in calm water, while for  $F_n=0.2$ , the tendency of duct's effect seems poor in waves in contract with the reduction effect on wake fraction in calm water. At  $L/\zeta=64.96$  and  $F_n=0.2$ , the effect of duct on wake fraction oscillates with wave length: for  $\lambda /L \leq 1$  and  $\lambda /L \geq 1.5$ , the duct lowers the wake fraction, but when  $1.0 \leq \lambda /L \leq 1.5$ , the duct increases the wake fraction. This oscillation in duct's effect may be due to random nature of more chaotic evolutions of vortices and instability of wake field at with higher carriage speed [20] and more specific studies are required to perform.
3. The duct's effect on relative rotative efficiency is very small (within 6%), and nearly no change with various wave conditions. This effect is proved experimentally by Nakamura and Natio [4].

### 3.7 The duct's effect on added power

Since the model keeps constant speed towing by the carriage with two velocities, there is no speed loss. But due to added resistance in waves, extra power is needed to deliver to the propeller in order to maintain constant forward speed. And this extra required power is called added power. The definition of added power is given as

$$\Delta P_D = \Delta(2\pi nQ) = (2\pi nQ)_{wave} - (2\pi nQ)_{calm} \quad (3.26)$$

where  $n$  and  $Q$  are propeller rotational speed and torque at self-propelled points.

To make up the deviation of deliver power  $\Delta P_{D\_change}$  caused by changing

self-propulsion point for certain tests when applying the interpolated method, a new method of calculating the deviation of deliver power is considered and the relevant equations are shown as following:

$$\Delta P_{D\_change} = (\Delta F_{D\_change})V_S / \eta_D \quad (3.27)$$

The relationship between effective power  $P_E$  and deliver power  $P_D$  is written as:

$$P_E = P_D \eta_D \quad (3.28)$$

The definition of effective power of model tests is expressed as:

$$P_E = (R_T - F_D)V_S \quad (3.29)$$

The details of change of deliver power and final corrected deliver power are shown as **Table 3.15**. Non-dimensional form of added power  $\Delta P\%$  is the ratio of added power in waves over deliver power in calm water at self-propulsion point. The non-dimensional form of corrected added power is written as:

$$\Delta P_{D\_change}\% = (\Delta P_{D\_change} / P_{calm}) \quad (3.30)$$

**Table 3.15** Correction of added power due to deviation of tow rope force

Test no.	Interpolated results		Correction to interpolation			sum
	$\Delta P$	$\Delta P\%$	$\Delta F_d$	$\Delta P_{D\_change}$	$\Delta P_{D\_change}\%$	
2332	64.28	2.08	38.77	93.17	3.02	5.11
2333	63.98	2.07	39.33	98.51	3.19	5.27
2334	63.56	2.06	37.23	88.02	2.85	4.92
2340	211.42	6.86	58.00	170.23	5.52	12.38
2010	3.79	0.11	35.46	95.37	2.81	2.93
2020	4.41	0.13	17.24	33.56	0.99	1.12
2030	3.30	0.10	63.78	182.18	5.37	5.47
2031	108.22	3.19	20.30	51.33	1.51	4.71
2040	108.63	3.20	84.45	231.68	6.83	10.04
2050	109.39	3.23	15.87	42.51	1.25	4.48
2210	46.83	3.95	14.81	21.17	1.78	5.73
2230	47.12	3.97	30.41	41.96	3.53	7.50
2240	46.10	3.88	90.29	151.25	12.74	16.62
2250	47.29	3.98	10.88	14.67	1.24	5.22
2130	74.40	5.94	16.43	22.39	1.91	7.84
2140	73.10	5.84	74.99	122.32	10.41	16.24

For each test, at different propeller rotational speed, tow rope force varies but

resistance keeps constant. Hence, it is the change of tow rope force that contributes to change of deliver power assuming quasi-propulsive coefficient  $\eta_D$  is identical for same wave condition, which is needed to be clarified.

The results of added power for open and ducted propeller varying with waves are presented and the comparisons of interpolated results and corrected results considering the change of tow rope force are shown from *Figure 3-28* to *Figure 3-32*.

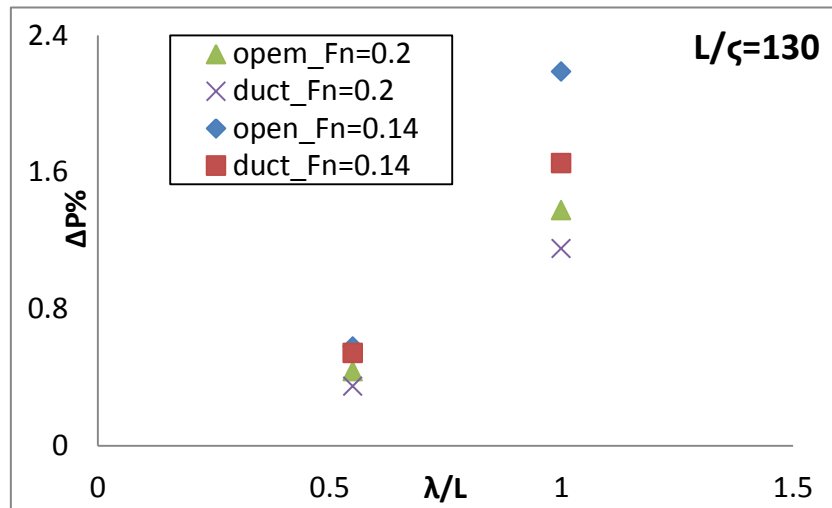


*Figure 3-28* The effect of wave length on added power at  $L/\zeta=130$

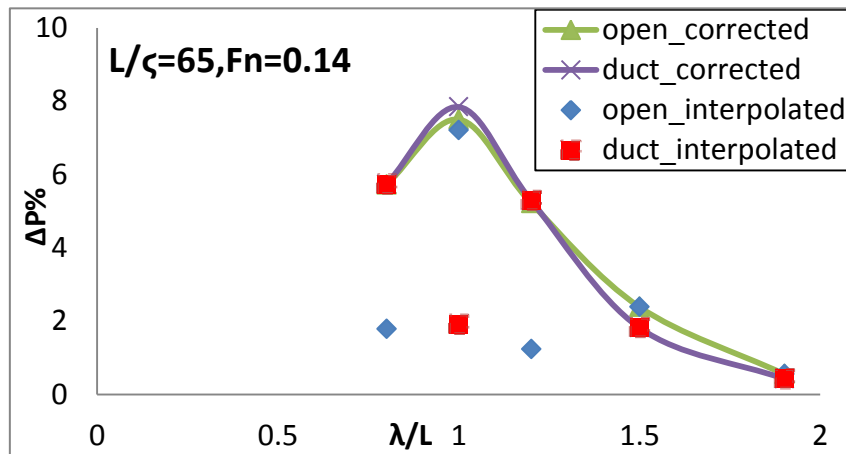


*Figure 3-29* The effect of wave length on interpolated results and corrected results at  $F_n = 0.14$

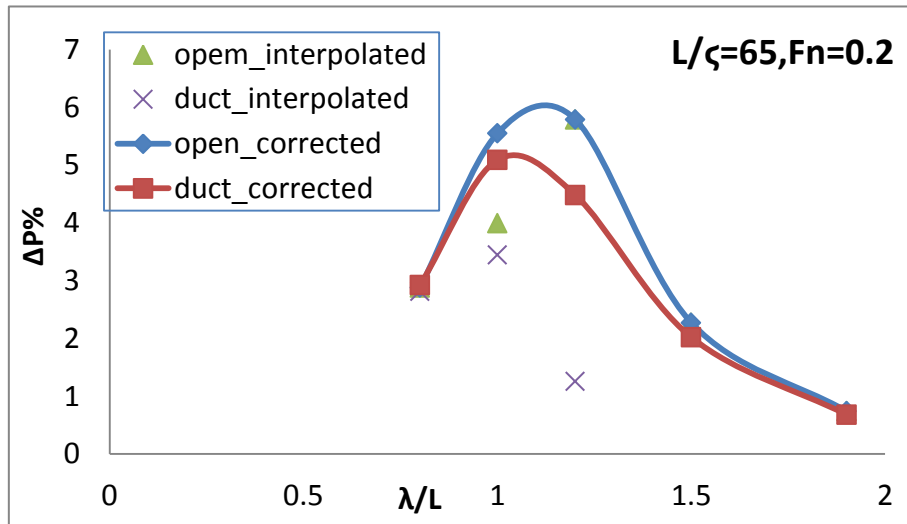


**Figure 3-30** The effect of wave length on interpolated results and corrected results at  $F_n = 0.20$

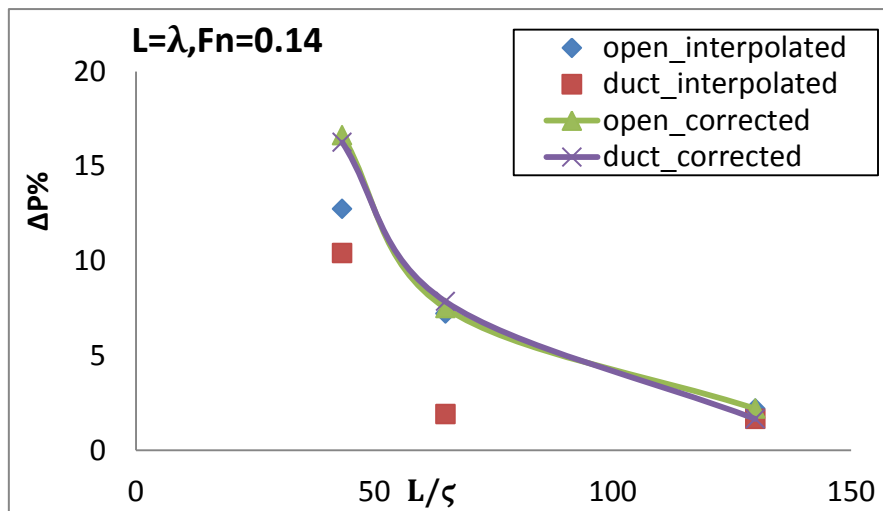


**Figure 3-31** The effect of wave height on interpolated results and corrected results at  $F_n = 0.14$

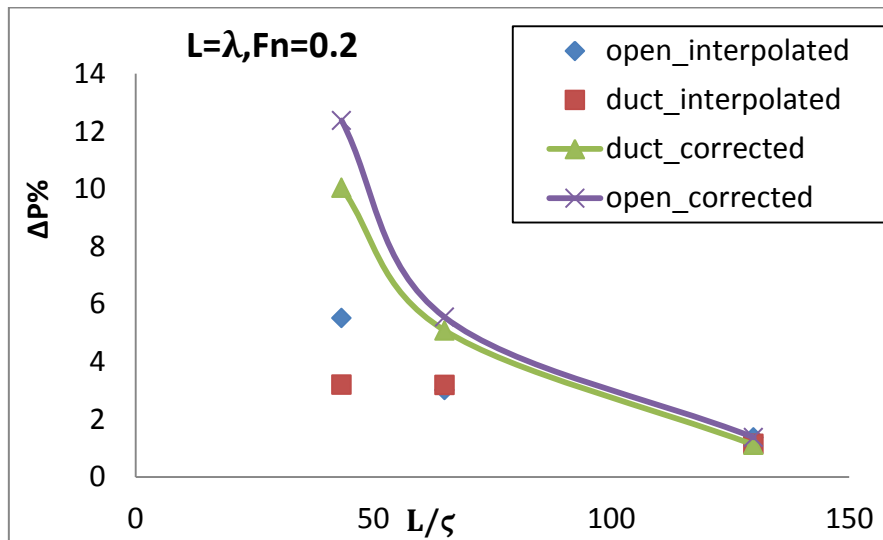


**Figure 3-32** The effect of wave height on interpolated results and corrected results at  $F_n = 0.20$

The curves of corrected data are smoother and reasonable when  $0.8 < \lambda/L < 1.5$ . But it is not sure that if this method gives more precise power prediction, because the quasi-propulsive coefficient is not identical for different propeller loading.

But to analysis of the duct's effect on added power, corrected data are used. The presence of the duct leads to added power varying with wave conditions and this effect is expressed by  $\Delta P_{duct}\%$ , which is the deviation of added power between open and ducted propeller over the added power for open propeller.

$$\Delta P_{duct}\% = \left( \frac{\Delta P_{D_{duct}} - \Delta P_{D_{open}}}{\Delta P_{D_{open}}} \right) \times 100\% \quad (3.31)$$

And comparisons between the results of interpolation method and correction method are shown in figures as follows:

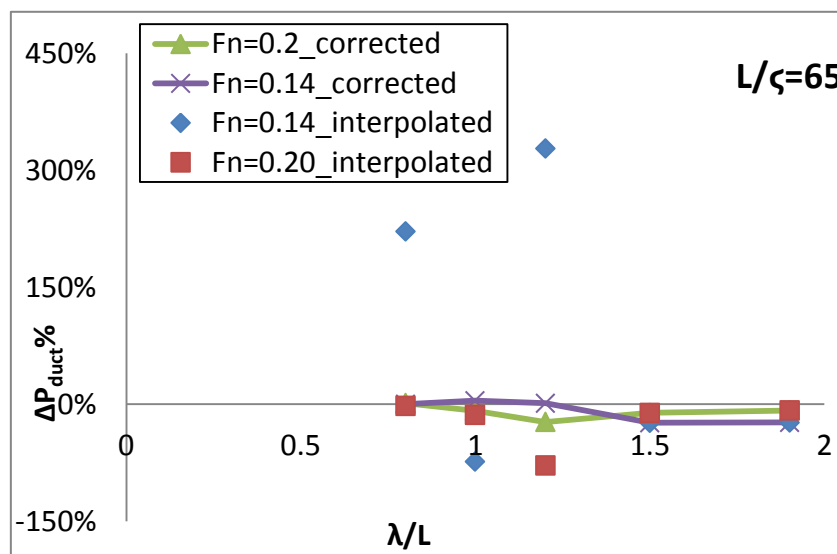


**Figure 3-33** The duct's effect on added power varying with wave periods

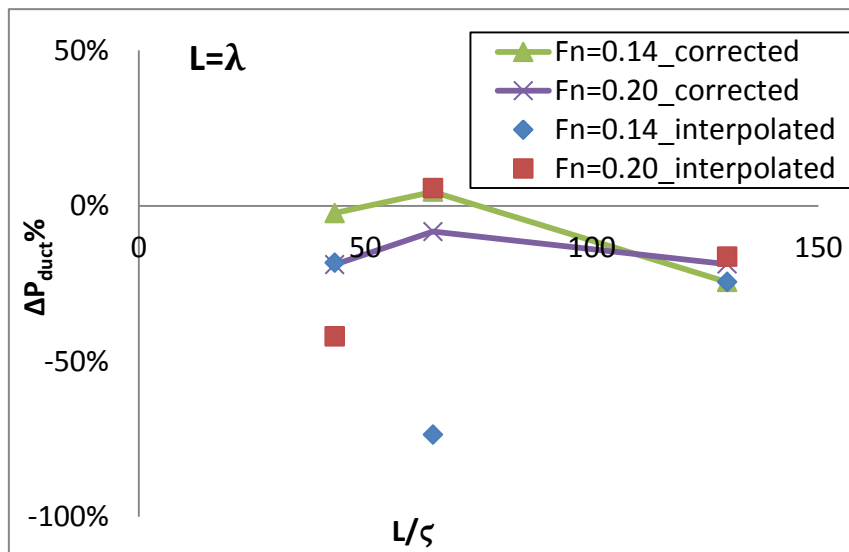


**Figure 3-34** The duct's effect on added power varying with wave amplitude

From the figures, the duct's effect on added power using corrected results show less striking as the interpolated results presented. Regardless of the difference between corrected data and interpolated data, the general tendency of the effect of the duct on added power is:

1. At  $L/\zeta = 64.96$ , the duct leads reduction on added power. For  $\lambda/L \geq 1.5$ , the duct's effect narrows with increasing wave period.
2. At  $\lambda/L = 1$ , the duct's effect on reducing the added power changes with wave height and is more dependence of forward speed. The tendency shows that the duct's influence on decreasing added power enlarges with smaller wave height of  $L/\zeta \geq 64.96$ .

### 3.8 The propeller's loading on wake fraction and propulsive efficiency

The method of using maximum RPS from the experimental data rather than extrapolation of RPS also induces large uncertainty. Due to change of propulsion points, the propulsive efficiency is affected by different propeller loading conditions. Hence, it is of great interest to see the effect of propulsor loading on wake fraction which shows the remarkable variance with wave conditions in figures of propulsive factors above.

Here the propeller loading coefficient [1] is defined as

$$C_T = T / (\frac{\rho}{2} V_a^2 \pi r^2) \quad (3.32)$$

where  $T$  is the propeller thrust for open propeller and total thrust for ducted propeller.  $V_a$  is advance speed of the model.  $r$  is propeller radius.

To analyze the propeller loading on wake fraction, propeller rotational speed is used instead of propeller loading coefficient to represent the propeller loadings. The effect of propeller loading on wake fraction and propeller efficiency for model with ducted propeller at  $F_n = 0.14$  is respectively presented as *Figure 3-35* and *Figure 3-36*.

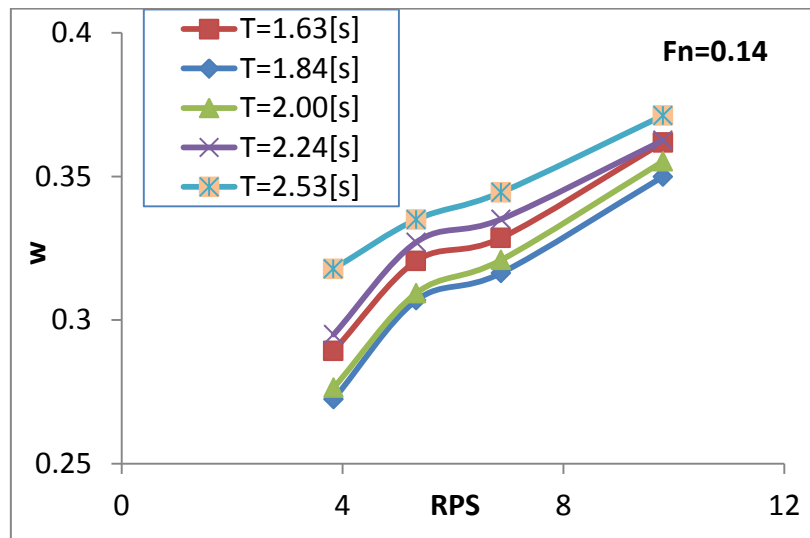


*Figure 3-35* The effect of RPS on wake fractions varying with waves at  $F_n = 0.14$

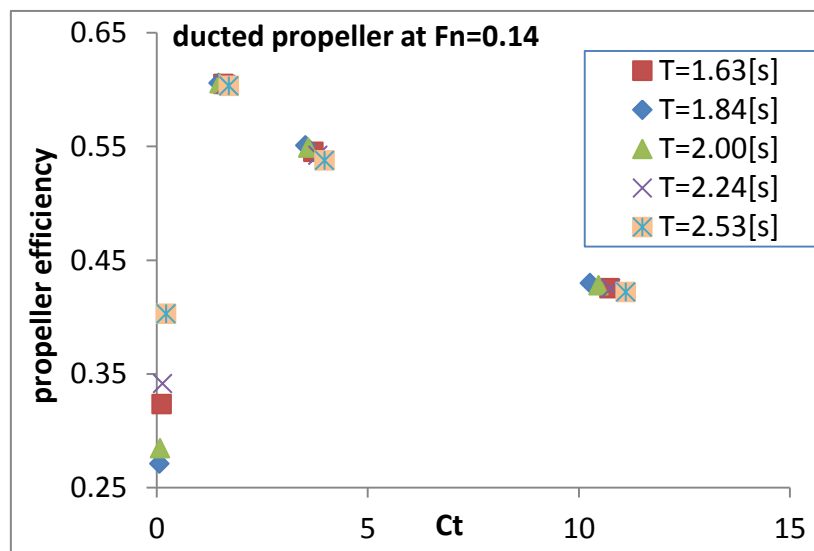


*Figure 3-36* The effect of propeller loading on propeller efficiency varying with waves



---

Seen from the figures, the effective wake increases with varying propeller rotational speed, and tendency of rise are identical for 5 wave periods.

Generally the propeller efficiency at first increases fast with propeller loading, after reaching maximum values, the propeller efficiency decrease relatively flat with larger propeller loading.

## 4. Comparisons of SHIPX and experimental results

### 4.1 RAO for motion variables

For comparisons of the experimental and numerical results, non-dimensional values are applied. For each model test, standard deviation of motion variables are read from manually selected time series of recorded data and by dividing the relevant standard deviation or wave slope of calibrated waves, RAO for motions are obtained in order to compare with non-dimensional numerical data which is calculated based on full scale ship model. The definitions of RAO for motions in SHIPX and for experimental data are listed as *Table 4.1*

**Table 4.1** RAO definitions in SHIPX and in experimental results

Method	RAO( $\eta_3$ )	RAO( $\eta_5$ )	RAO( $\ddot{\eta}_3$ )
SHIP-X	$\frac{\eta_3}{A}$	$\frac{\eta_5}{kA}$	$\frac{\ddot{\eta}_3}{gA}$
Experimental results	$\frac{\sigma_{\eta_3}}{\sigma_{wave}}$	$\frac{\sigma_{\eta_5}}{k\sigma_{wave}}$	$\frac{\sigma_{\ddot{\eta}_3}}{\Lambda g\sigma_{wave}}$

For pitch motion, the definition of RAO is expressed as

$$\text{RAO}(\eta_5) = \eta_5 / kA_d \quad (4.1)$$

And  $k$  is wave number for regular waves:

$$k = (2\pi/T)^2 / g. \quad (4.2)$$

It is noting that for acceleration there is no scale effect concerning Froude scaling. So when transferring acceleration into non-dimensional value, it is divided by product of wave amplitude and acceleration of gravity in SHIPX, however, if standard deviation of wave for model tests is applied to get RAO for experimental data, there leads to length scaling. To make up this scaling, standard deviation of wave is multiplied by  $\Lambda = 22.629$ .

The comparisons of non-dimensional experimental and numerical results are plotted into figures. It is noting that in the following figures, ‘nu’ refers to numerical results and ‘ex’ represents experimental results.

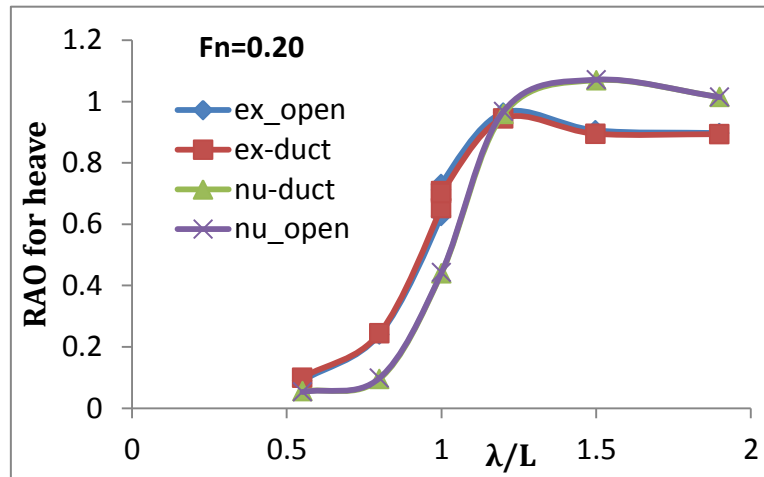


**Figure 4-1** Comparisons of RAO for heave from SHIPX and experimental results with varying wave length at  $F_n = 0.2$

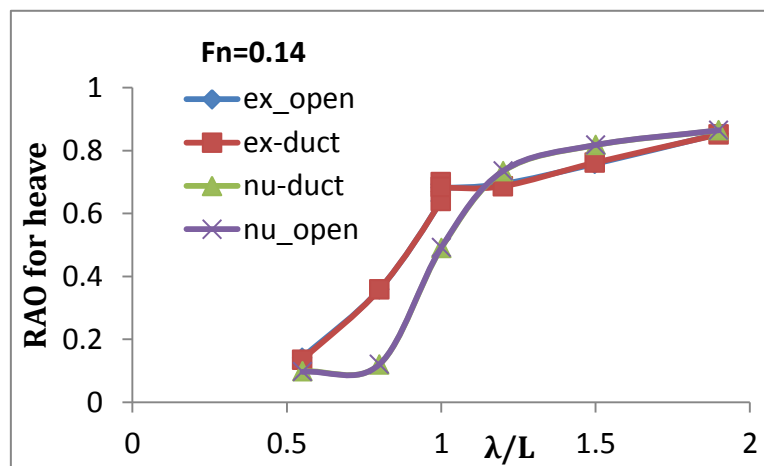


**Figure 4-2** Comparisons of RAO for heave from SHIPX and experimental results with varying wave length at  $F_n = 0.14$

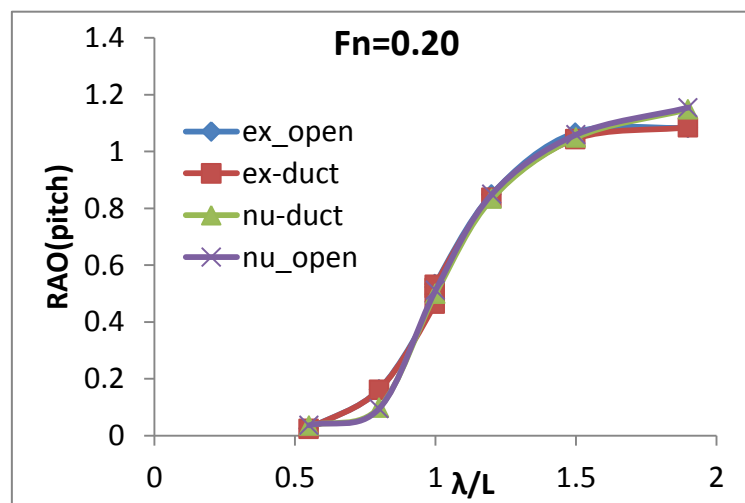


**Figure 4-3** Comparisons of RAO for pitch from SHIPX and experimental results with varying wave length at  $F_n = 0.20$

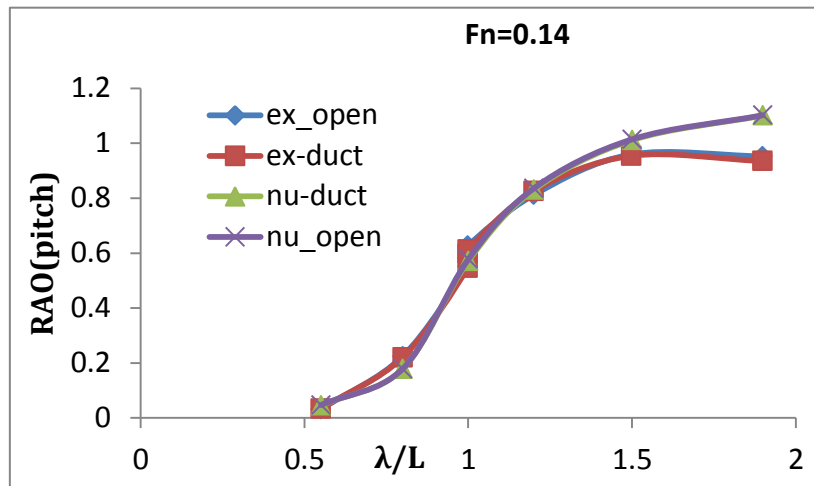


**Figure 4-4** Comparisons of RAO for pitch from SHIPX and experimental results with varying wave length at  $F_n = 0.14$

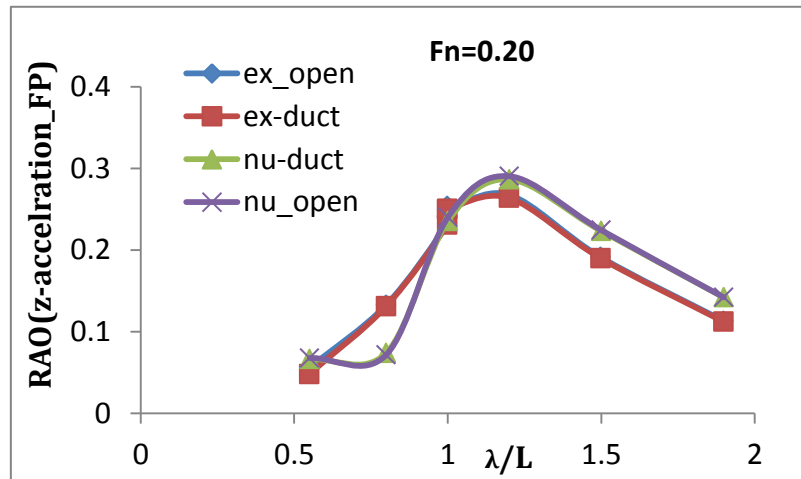


**Figure 4-5** Comparisons of RAO for acceleration at FP from SHIPX and experimental results with varying wave length at  $F_n = 0.20$

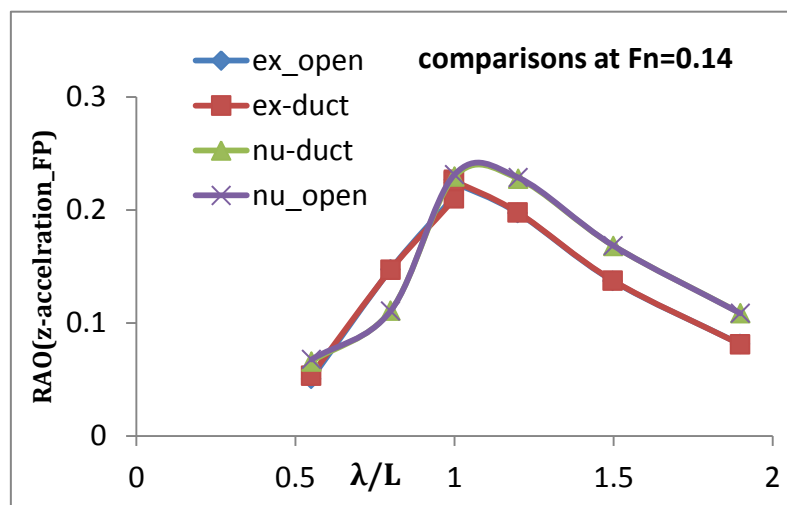


**Figure 4-6** Comparisons of RAO for acceleration at FP from SHIPX and experimental results with varying wave length at  $F_n = 0.14$

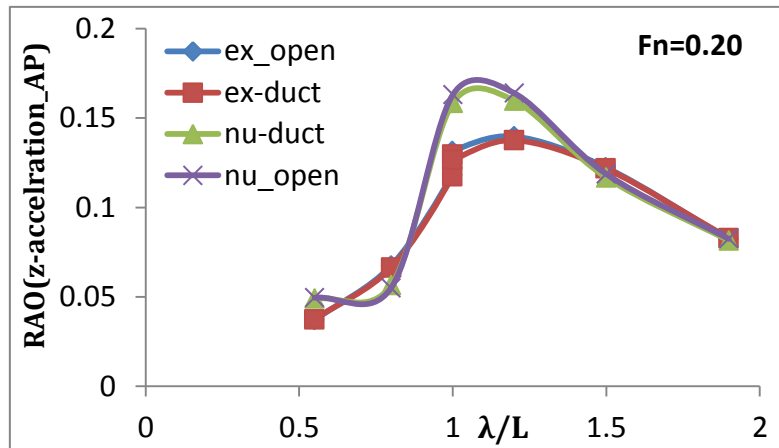


**Figure 4-7** Comparisons of RAO for acceleration at AP from SHIPX and experimental results with varying wave length at  $F_n = 0.20$

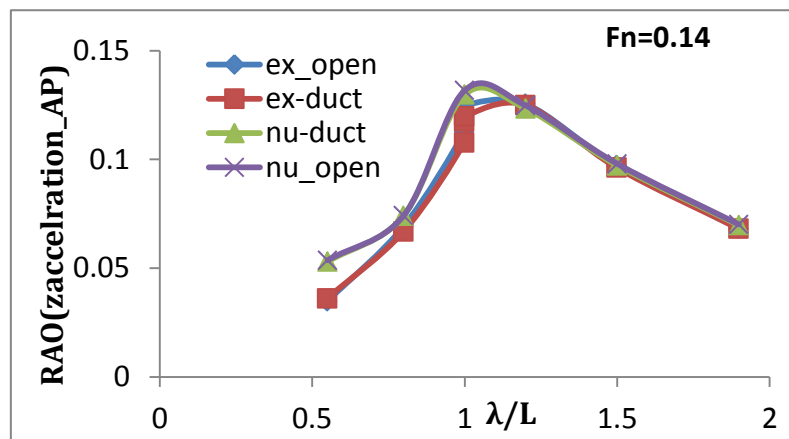


**Figure 4-8** Comparisons of RAO for acceleration at AP from SHIPX and experimental results with varying wave length at  $F_n = 0.14$

For heave motion, the maximum deviation between the experimental and numerical result takes place at  $\lambda/L = 08$  for both velocities. The experimental results are larger within the range of  $\lambda/L < 1.2$ , but with increasing wave length, the deviation narrows and the numerical results are a bit larger than experimental ones. When  $\lambda/L \geq 2$ , the deviation becomes neglected.

The numerical and experimental results of RAO for pitch motion give very good match for both velocities and the maximum deviation is less than 6% for smaller velocity of  $F_n = 0.14$  around  $\lambda/L = 2$ . For vertical acceleration measured at FP, when  $\lambda/L < 1$  the general tendency of deviation between numerical and experimental results shows similarly as that of heave motion. But with longer waves of  $\lambda/L \geq 1$ , the deviation enlarges with increasing wave length and smaller velocity

For vertical acceleration measured at AP, generally the numerical results are bit slightly larger compared with experimental results. The exception occurs around  $\lambda/L = 1$ , where the deviation goes to 16%.

## 4.2 Non-dimensional added resistance

The comparisons of numerical and experimental results on non-dimensional added resistance are shown as:

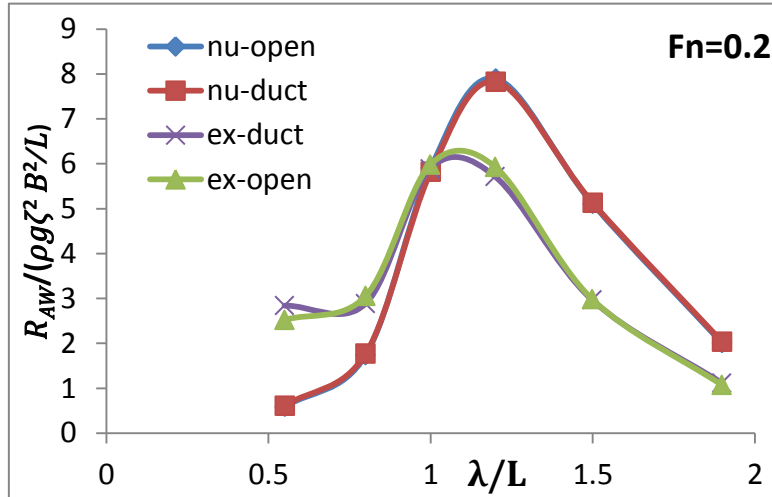


**Figure 4-9** Comparisons of added resistance from SHIPX and experimental results with varying wave length at  $F_n = 0.2$

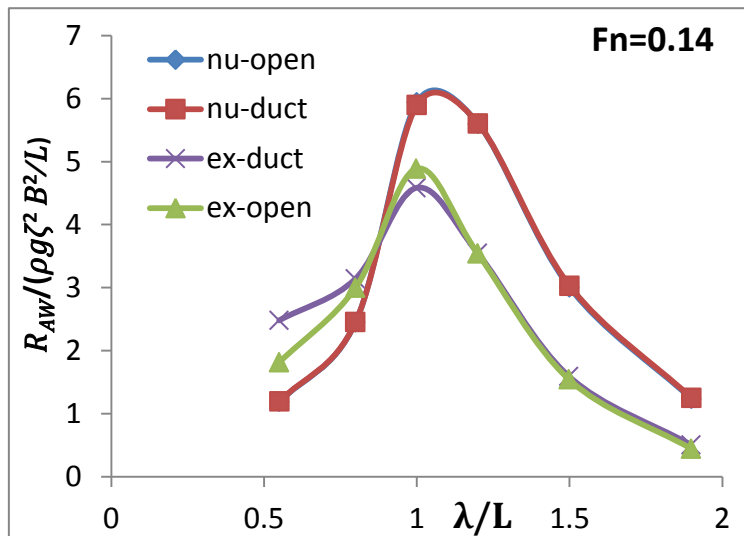


**Figure 4-10** Comparisons of added resistance from SHIPX and experimental results with varying wave length at  $F_n = 0.2$

The general tendency of deviation between numerical and experimental results of added resistance is very alike that of vertical acceleration measured at FP. For waves of  $\lambda/L < 1$ , the experimental data are larger, but this deviation narrows with increasing wave length and higher speed. For waves of  $\lambda/L \geq 1$ , the deviation rises with increasing wave length and smaller speed.

### 4.3 Augment of added power

First interpolated results without correction of the model tests are compared with numerical data in *Figure 4-11* and *Figure 4-12*.

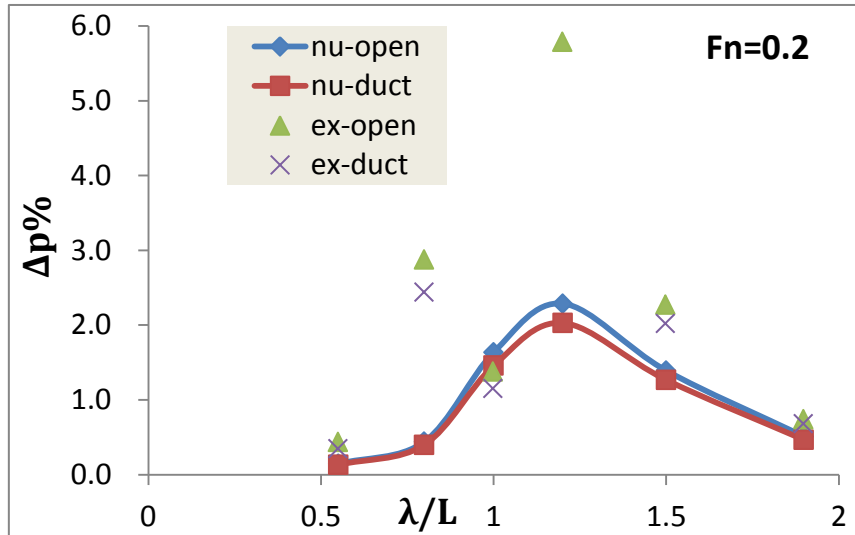


*Figure 4-11* Comparisons of added power from SHIPX and interpolated experimental results with varying wave length at  $F_n = 0.2$

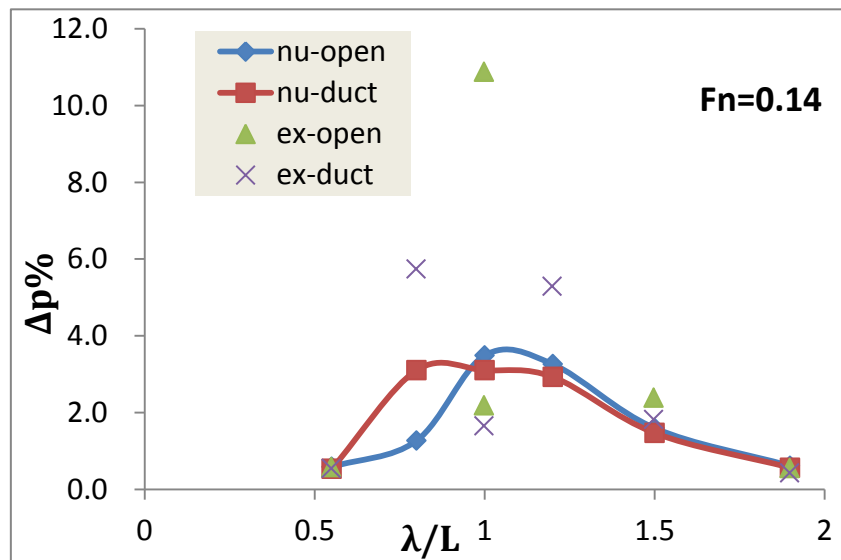


*Figure 4-12* Comparisons of added power from SHIPX and interpolated experimental results with varying wave length at  $F_n = 0.2$

The comparisons of corrected results from model tests (shown with “\_c”), with interpolated results from the model tests (for sub of ‘inter’) and numerical results from SHIPX are plot as *Figure 4-13* and *Figure 4-14*.

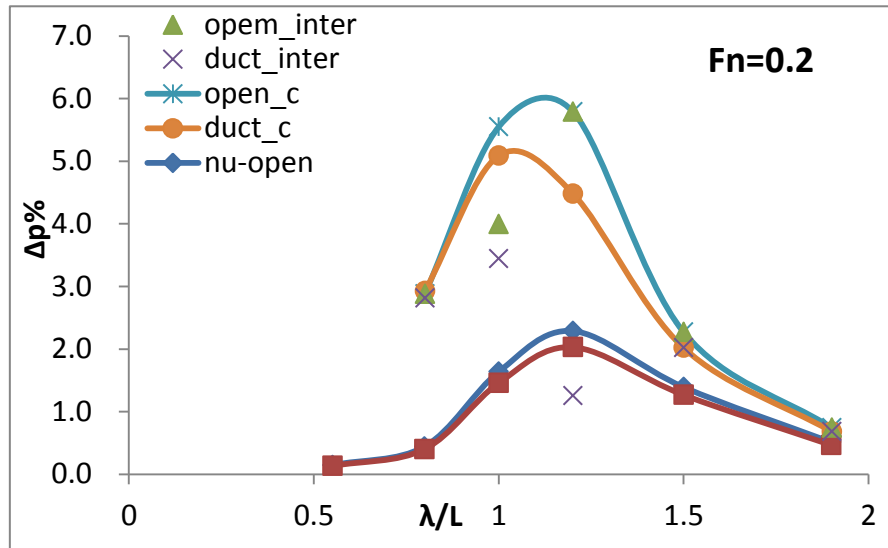


**Figure 4-13** Comparisons of added power from SHIPX and experimental results by interpolated method and by final correction results with varying wave length at  $F_n = 0.2$

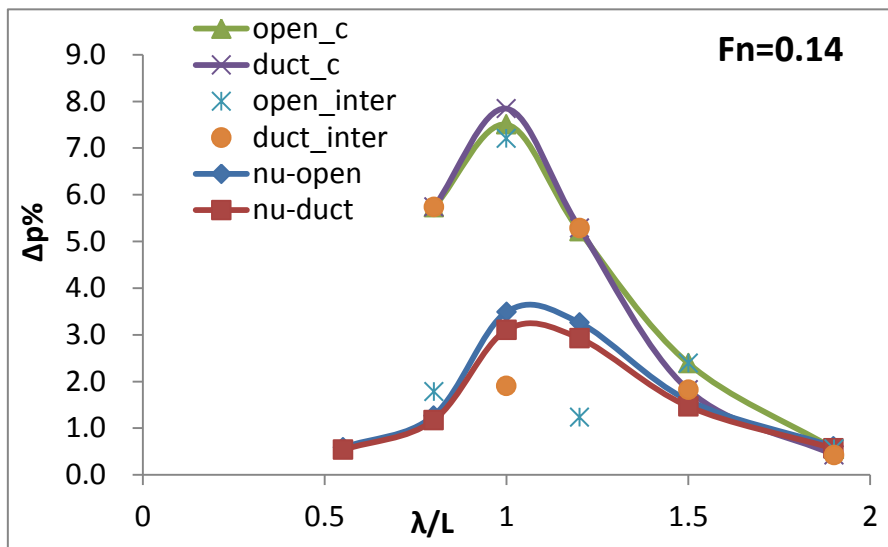


**Figure 4-14** Comparisons of added power from SHIPX and experimental results by interpolated method and by final correction results with varying wave length at  $F_n = 0.14$

For comparisons of added power, the deviation between numerical and experimental results is most remarkable under the critical conditions at  $\lambda/L = 1$  and  $\lambda/L = 1.2$  respectively for two velocities of  $F_n = 0.14$  and  $F_n = 0.20$ . For  $0.8 < \lambda/L < 1.2$  the experimental data based on interpolated method give incredible values compared with numerical data.



## 5. Conclusion and further work

Numerical and experimental investigations into the duct's effect on ship's motion and speed loss are presented in this work. The following conclusions can be drawn:

1. Both experimental and numerical results show that the duct's presence produces general tiny deviation in RAOs for motion variables. The deviation of RAOs for motion variables limits within 5% for results obtained from SHIPX for all wave periods. The exception comes from the analysis of experimental results, at shortest wave  $\lambda/L = 0.55$ , the variations of motion variables show most remarkable and depend on forward speed. The duct's effect on RAOs for motion variables can be neglected when  $\lambda/L \geq 1$ . So the benefit of using a ducted propeller for sea-keeping performance is not promising.
2. As for the duct's effect on added resistance, the experimental results are much more impressive compared with the numerical ones, the latter shows similar tendency but much smaller (limited within 5%) deviation for all wave periods. The analysis of the experimental results presents that at shortest wave of  $\lambda/L = 0.55$ , the duct promotes almost 40% more added resistance at smaller velocity  $F_n = 0.14$ ; when  $0.8 < \lambda/L < 1.2$ , the duct leads relatively tiny decrease.
3. The duct's effect on added power based on numerical and experimental data are not very matched. This due to the shortcomings of interpolated method and correction methods.
4. For results obtained from SHIPX, the presence of the duct leads to a reduction on added power for all wave period. The duct's effect of reduction on added power shows most remarkable around  $\lambda/L = 1$  and lessens with increasing wave length. And at smaller forward speed, the duct's effect is more impressive. For experimental analysis of added resistance, the duct's effect is function of wave height and wave period. The tendency shows that the duct's influence on decreasing added power enlarges with smaller wave height of  $L/\zeta \geq 64.96$ . Hence the advantage of using a ducted propeller on speed loss needs more studies experimentally.
5. The wake fraction in regular waves oscillates considerably with wave height and wave period, in particular in the range of  $0.8 < \lambda/L < 1.2$ .
6. The presence of the duct results in more variance of relative rotative efficiency in waves from the calm water results at smaller velocity; and the duct leads a decrease on deviation of wake fraction in waves and in calm water, this effect rises at smaller velocity.
7. The propeller loading have effect on wake fraction and propeller efficiency and

---

this effect changes with wave conditions. The effective wake increases with varying propeller rotational speed, and tendency of rise are identical for 5 wave periods. the propeller efficiency tends to increases rapidly at first with propeller loading, after reaching maximum values, the propeller efficiency decrease relatively flat with larger propeller loading

Further studies about the duct's effect are needed:

1. This thesis considers the duct's effect in regular waves while real sea states are harsher, so the duct's effect in irregular waves or oblique waves should be investigated.
2. For model tests, higher RPS values should be included to reach designed tow rope force and to give more precise power predictions. The data processing method should be improved since the interpolated method induces large uncertainty.
3. Duct's effect on wake fraction and relative rotative efficiency are needed more analysis, because propulsive factor are very important to power predictions. SHIPX calculations give no information about real wake field so CFD method is required to find details of information about wake field.

---

## Reference

1. Carlton, J., "Marine propellers and propulsion ", Butterworth-Heinemann , 2007
2. Sacks, A.H., and Burnell, J.A., "Ducted propeller-a critical review of the state of art", Technical Information Agency Report No. ARD-232, Virginia, 1959, page 5-6,
3. Celik, F.,Guner, M., and Ekinici, S., "An approach to the design of ducted propeller", Transactions, Mechanical Engineering Vol. 17, No. 5, pp. 406-417, 2010
4. Nakamura,S. and Natio,S., "Propulsive performance of a container ship in waves", The Society of Naval Architects of Japan. Naval Architecture and Ocean Engineering Vol.15, 1977.
5. Faltinsen, O. M., Minsaas, K. J., Liapias, N. and Skjrdal, S. O. (1980). "Prediction of resistance and propulsion of a ship in a seaway". In 13-th Symp. Naval Hydrodynamics, Tokyo
6. Seakeeping Performance of Ships (projekt)., Nordforsk, "Assessment of ship performance in a seaway", Nordforsk,1987,chapter 4.3,page 26
7. Morgan, W.B., and Caster, E.B., "Prediction of the aerodynamic characteristics of annular airfoils", Hydromechanics Laboratory Research and Development Report, report no.1830, January 1965
8. Van Manen ,J.D., Oosterveld, M.W.C. "Series of model tests on ducted propellers", report under contract No. N62558-3960, Netherlands Ship Model Basin, Wageningen, The Netherlands (1972)
9. Falcao de Campos, J. A. C. "On the calculation of ducted propeller performance in axisymmetric flows", Delft, Technische Hogeschool, Doctor in de technische Wetenschappen Thesis, 1983
10. Barros E.A., Dantas J.L.D., "Effect of a propeller duct on AUV maneuverability ", Ocean Engineering 42, pp.61 - 70, 2012
11. Chuang,Z. and Steen,S. "Experimental and numerical study of stem shape influence on speed loss in waves", Ship Technology Research Schiffstechnik Vol. 59, No. 2, pp. 4-17, April 2012
12. Fathi, D., and Hoff, J.R, "SHIPX vessel response", Theory manual. MARINTEK.
13. Capt. Dipl. -Ing.J.Brix, "Maneuvering technical manual", Seehafen Verlag GMBH, Hamburg, 1993, pp.67-69
14. Faltinsen, O.M., "Hydrodynamics of high-speed marine vehicles", Cambridge University Press, 2005, pp187-193
15. Fletcher, H.S., "Experimental investigation of lift, drag, and pitching moment of five annular airfoils", NACA technical note 4117, Langley Aeronautical

---

Laboratory, 1957

16. Hoerner, S. F., and Borst, H. V., "Fluid-dynamic lift: practical information on aerodynamic and hydrodynamic lift ", Hoerner Fluid Dynamics, 1985.
17. Coleman, H.W., and Steele, W. G., "Experimentation, validation, and uncertainty analysis for engineers", John Wiley & Sons, 3rd edition, 2009
18. Faltinsen, Odd M., "Sea loads on ships and offshore structures", Society of Naval Architects of Korea 1999
19. Guo B.J., "Numerical and experimental investigation of added resistance in waves", NTNU, Doctor thesis in Marine Technology, 2011
20. Felli, M., Camussi, R., and Difelice, F., "Mechanisms of evolution of the propeller wake in the transition and far field." *Journal of Fluid Mechanics*, Volume 682, September 2011, pp. 5-53

## Appendix A: calculation of flat plate

Based on reference [7] [15] [16] the area of flat plate is calculated by two methods as following:

### 1. Resource 1

A family of annular airfoil with same projected area (equals to product of inner diameter and chord parallel to center line) was referred. Different aspect ratio corresponds to different lift curves and the data of interest are list in **Table A.0.1**. It is noted that the definition of the aspect ratio for the foil in NACA paper is

$$\Lambda = d/c \quad (A.0.1)$$

**Table A.0.1** Lift coefficient at three angles of attack [15]

Aspect ratio	Lift coefficient at three angle of attack		
	0°	5°	10°
1.0	0	0.25	0.50
1.5	0	0.35	0.70
3.0	0	0.50	1.00

It is noting that the aspect ratio based on *Equation (A.1)* is 1.05. The data is shown as **Table A.0.2**

**Table A.0.2** Lift coefficient for aspect ratio of 1.05 [7]

Aspect ratio $d/c$	Lift coefficient at three angle of attack		
	0°	5°	10°
1.05	0	0.27	0.50

Interpolate lift coefficient for the duct with aspect ratio of 2 from **Table A.0.1** and **Table A.0.2**. The results are presented in **Table A.0.3**.

**Table A.0.3** Lift coefficient for aspect ratio of 2

Aspect ratio $d/c$	Lift coefficient at three angle of attack		
	0°	5°	10°
2	0	0.40	0.80

If flat plate in two-dimensional steady flow with infinite fluid is considered and based on potential flow theory the lift coefficient is expressed as:

$$C_L = 2\pi\alpha \quad (\text{A.0.2})$$

Hence the area of flat plate becomes  $6.43[\text{m}^2]$ . However, the ideal model is not very applicable since infinite fluid boundary is not satisfied.

While refer to NACA paper [7], it is concluded that the lift curve slope of annular foil is approximately twice of slope for lift curve for rectangular plane airfoil with same aspect ratio. The slope of lift curve for annular foil can be expressed as:

$$\frac{dC_L}{d\alpha} = \frac{0.8-0.4}{(10-5) \times \frac{2\pi}{360}} = 4.58 \quad (\text{A.0.3})$$

Set aspect ratio of 2 for flat plate, the lift curve slope is 2.29. The corresponding lift coefficients for flat plate are list as **Table A.0.4**.

**Table A.0.4** Lift coefficients for flat plate with lift curve slop of 2.29

Aspect ratio $d/c$	Lift coefficient at three angle of attack		
	$0^\circ$	$5^\circ$	$10^\circ$
2	0	0.20	0.40

Finally the dimensions for flat plate can be calculated and list as **Table A.0.5**.

**Table A.0.5** Dimensions for flat plate based on resource 1

Length of span [m]	5.94
Length of chord[m]	2.97
Projected area[ $\text{m}^2$ ]	17.64

## 2 Resource 2

Alternatively, from [16] it indicates the effective wing area of a ring equals

$$S = 0.5\pi dc \approx 1.6dc \quad (\text{A.0.4})$$

Here the definition of the aspect ratio is different in [16]:

$$\Lambda = 2d^2/S = 4d/\pi c \quad (\text{A.0.5})$$

Based on the given geometry of ring foil, the ratio  $d/c$  equals to 3.28.

And induced angle is expressed as:

$$\frac{d\alpha}{dC_L} = \frac{1}{\pi A_i} = 0.25 \frac{c}{d} \quad (\text{A.0.6})$$

Thus the relationship between total lift angle and lift coefficient is written as

$$\frac{d\alpha}{dC_L} = \left( \frac{0.5}{0.8\pi} \right) + \left( \frac{1}{\pi A_i} \right) = 0.2751 \quad (\text{A.0.7})$$

For linearity relationship between lift coefficient and angle of attack, it is shown

$$C_L = \frac{1}{0.275} \alpha = 3.6364\alpha \quad (\text{A.0.8})$$

So lift coefficient at lift angle of  $5^\circ$  and  $10^\circ$  can be obtained as **Table A.0.6**.

**Table A.0.6** Lift coefficients for ring foil with  $d/c$  ratio of 3.28

Ratio $d/c$	Lift coefficient at three angle of attack		
	$0^\circ$	$5^\circ$	$10^\circ$
3.28	0	0.32	0.64

Since data is limited under only one situation for  $d/c = 3.28$ , it is rough guessing to choose lift coefficient for  $d/c = 2.0$ . Otherwise it is permissible to use data of  $d/c = 3.28$  as upper limit for projected area for flat plate. Similarly two equations for angle  $5^\circ$  and  $10^\circ$  were formed respectively, but it is noting the effective area for foil is different for ring foil instead of the product of chord and diameter.

The area of flat plate based on a ring foil with  $d/c$  ratio of 3.28 can be obtained. The dimensions are shown as

**Table A.0.7** dimensions for flat plate based on model 2

Length of span [m]	6.72
Length of chord[m]	3.36
Projected area[m <sup>2</sup> ]	22.58

# Appendix B: numerical results from SHIPX

## 1. Ship response analysis

The deviation of RAO for motion and added resistance between open propeller and ducted propeller are calculated as *Equation (B.0.1)* and list in **Table B.0.1** and **Table B.0.2**.

$$\Delta\eta_{duct} = \frac{\eta_{duct} - \eta_{open}}{\eta_{open}} \times 100\% \quad (\text{B.0.1})$$

Here  $\eta$  represents the ship motion variables for heave, pitch and vertical accelerations as well as added resistance.

**Table B.0.1** The duct's effect on motions and acceleration for 5 wave periods

$\Delta\eta\%$	$\eta_3$		$\eta_5$		$\ddot{\eta}_{3\_AP}$		$\ddot{\eta}_{3\_FP}$	
	$F_n = 0.14$	$F_n = 0.20$	$F_n = 0.14$	$F_n = 0.20$	$F_n = 0.14$	$F_n = 0.20$	$F_n = 0.14$	$F_n = 0.20$
1.90	-0.06%	0.02%	-0.10%	-0.50%	-0.53%	-1.15%	0.13%	-0.09%
1.50	-0.07%	-0.17%	-0.30%	-0.94%	-0.79%	-1.66%	-0.07%	-0.51%
1.20	-0.21%	-0.85%	-0.65%	-1.86%	-1.15%	-2.55%	-0.41%	-1.38%
1.00	-0.44%	-0.68%	-1.04%	-2.38%	-1.49%	-2.86%	-0.81%	-1.93%
0.80	-0.31%	-3.45%	0.16%	3.38%	-0.05%	2.71%	0.26%	3.11%
0.55	1.83%	3.87%	-2.53%	-2.16%	-1.19%	-1.13%	-2.63%	-2.19%

And the duct's effect on added resistance is shown as **Table B.0.2**.

**Table B.0.2** The duct's effect on added resistance

$\lambda/L$	$F_n = 0.14$	$F_n = 0.20$
1.90	1.2%	1.3%
1.50	0.8%	0.4%
1.20	0.0%	-0.9%
1.00	-0.7%	-1.5%
0.80	0.1%	1.9%
0.55	0.6%	3.8%

## 2. Added power and speed loss

The resistance data used in SHIPX for calm water performance for both open propeller and ducted propeller are listed as **Table B.0.3**.



**Table B.0.3** Resistance data

$V_S$ [knot]	$R_T$ [KN]
7	47.44
8	65.58
9	83.85
10	101.72
11	122.56
12	142.01
13	159.9
14	191.9
15	222.97
16	253.92

The comparisons of brake power for given speed and the deviation between the results of open propeller and ducted propeller are shown as **Table B.0.4** and **Table B.0.5**.the comparisons of attainable speed for given brake power are presented as **Table B.0.6**.

**Table B.0.4** Comparisons of added power for open propeller and ducted propeller

$\frac{\Delta P}{P_{calm}} = \frac{P_{wave} - P_{calm}}{P_{calm}}$		Open propeller		Ducted propeller	
$T$ [s]	$\lambda/L$	$F_n = 0.14$	$F_n = 0.20$	$F_n = 0.14$	$F_n = 0.20$
11.96	1.90	0.609	0.512	0.565	0.467
10.63	1.50	1.596	1.391	1.468	1.267
9.51	1.20	3.260	2.287	2.927	2.029
8.68	1.00	3.489	1.637	3.103	2.029
7.76	0.80	1.268	0.442	3.103	1.459
6.44	0.55	0.586	0.146	0.537	0.133

**Table B.0.5** The duct's effect on added power varying with wave periods

$T$ [s]	$\lambda/L$	$F_n = 0.14$	$F_n = 0.20$
11.96	1.90	-7.2%	-8.8%
10.63	1.50	-8.0%	-8.9%
9.51	1.20	-10.2%	-11.3%
8.68	1.00	-11.0%	23.9%
7.76	0.80	144.8%	230.0%
6.44	0.55	-8.4%	-9.3%

**Table B.0.6** The attainable speed for given brake power in calm water and in regular waves

Speed loss		$V_S$ [knot]		$\frac{\Delta V}{V_{calm}} = \frac{V_{wave} - V_{calm}}{V_{calm}}$	
$T$ [s]	$\lambda/L$	Open propeller	Ducted propeller	Open propeller	Ducted propeller
11.96	1.90	13.9	14.13	-12.081%	-11.355%
10.63	1.50	11.75	12.11	-25.680%	-24.028%
9.51	1.20	9.7	10.17	-38.646%	-36.198%
8.68	1.00	9.49	10.25	-39.975%	-35.696%
7.76	0.80	14.4	14.72	-8.918%	-7.654%
6.44	0.55	15.47	15.65	-2.151%	-1.819%
<i>calm</i>	1.90	15.81	15.94	-	-

## Appendix C: calculation of tow rope force at self-propulsion point

At self-propulsion point, the tow rope force equals to the correction for difference of frictional resistance and other effects such as correlation allowance, scale effect; so that in model tests propeller bears same loading as the ship propeller in full scale.

The formula to calculate tow rope force is expressed as

$$F_D = \frac{1}{2} C_{FD} \rho_M S_M V_M^2 \quad (C.0.1)$$

where index 'M' denotes model scale,  $\rho_M$  is water density,  $S_M$  is wetted surface,  $V_M$  is carriage speed.

The standard method applied in MARINTEK for  $C_{FD}$  tow rope force coefficient can be defined as

$$C_{FD} = (1 + k_0)(C_{FM} - C_{FS} - \Delta C_F) + (C_{BDM} - C_{BDS}) + (C_{APPM} - C_{APPS}) - C_A \quad (C.0.2)$$

With  $k_0$  is form factor; index 'S' refers to full scale variables,  $C_F$  is frictional resistance coefficient and  $\Delta C_F$  is roughness allowance for ship;  $C_{BD}$  is transom stern resistance coefficient;  $C_{APP}$  is appendage resistance coefficient.

For model tested without appendages and neglecting transom stern effects, tow rope force coefficient can be ideally simplified as

$$C_{FD} = (1 + k_0)(C_{FM} - C_{FS} - \Delta C_F) \quad (C.0.3)$$

The details of calculation for tow rope force are as following:

### 1. Form factor $k_0$

Form factor is function of dimensions of model and ship, according to the method recommended by MARINTEK, it can be obtained by

$$k_0 = 0.6\varphi + 75\varphi^3 \quad (C.0.4)$$

With

$$\varphi = \frac{C_B}{L_{WL}} \sqrt{(T_{AP} + T_{FP})B}. \quad (C.0.5)$$

So form factor is calculated as:

$$\begin{aligned} \varphi &= 0.0833784; \\ k_0 &= 0.0935 \end{aligned}$$

Form factor is identical for both model and full scale tests.

### 2. Frictional resistance coefficient for both model $C_{FM}$ and full scale $C_{FS}$ , and roughness $\Delta C_F$ . According to ITTC-57 correlation line, frictional resistance coefficient is given as

$$C_F = \frac{0.075}{(\log R_n - 2)^2} \quad (C.0.6)$$

where  $R_n$  is Reynolds number, and it is denoted as

$$R_n = \frac{VL_{WL}}{\nu} \quad (C.0.7)$$

Similarity of Froude number is used to get velocity for model scale. Assuming same gravity acceleration, model scale velocity is written as

$$V_M = \sqrt{\frac{L_S}{L_M}} \times V_S \quad (C.0.8)$$

And roughness allowance is expressed as

$$\Delta C_F = [110.31(H \times V_S)^{0.21} - 403.33] \times C_{FS}^2 \quad (C.0.9)$$

The details of calculated Reynolds numbers, frictional resistance coefficient and roughness allowance are shown in **Table C.0.2**.

3. Tow rope force  $F_D$  for given carriage speed Using *Equation (C.0.3)*, tow rope force is determined and listed as **Table C.0.3**.

**Table C.0.1** The data for ship and model

Variable	unit	full scale	model scale
Length on waterline $L_{WL}$	[m]	119.19	5.267
Breadth at waterline B	[m]	20.8	0.919
Draught $T_{AP}/T_{FP}$	[m]	5.5	0.243
Draught T at $L_{pp}/2$	[m]	5.5	0.243
Wetted surface S	[m <sup>2</sup> ]	2861.8	5.589
block coefficient $C_B$	[-]	0.657	0.657
Kinematic viscosity $\nu$	[m <sup>2</sup> /s]	1.19E-06	1.12E-06
water density $\rho$	[kg/m <sup>3</sup> ]	1025	1000
Hull roughness H	[ $\mu$ m]	150	[-]

**Table C.0.2** Calculation of Reynolds number, frictional resistance coefficient and roughness allowance

$V_S$ [knot]	$F_n$	$V_M$ [m/s]	$R_{nS}$	$C_{FS}$	$R_{nM}$	$C_{FM}$	$\Delta C_F$
9.4	0.14	1.016	4.84E+08	1.68E-03	4.78E+06	3.43E-03	1.03E-04
13.4	0.20	1.449	6.9E+08	1.60E-03	6.81E+06	3.21E-03	1.81E-04

**Table C.0.3** Tow rope force at self-propulsion point

$F_n$	$V_S$ [knot]	$V_M$ [m/s]	$F_D$ [N]
0.14	9.4	1.016	5.190
0.20	13.4	1.449	9.145

## Appendix D: results of propulsive factors

The data for interpolated propulsive factors for all tests are list as follows:

**Table D.0.1** The results of interpolated propulsive factors for open propeller at

$$F_n = 0.14$$

Open prop $F_n=0.14$	t	w	$\eta_r$
2200	0.109	0.575	0.977
2210	0.157	0.133	1.063
2220	0.108	0.509	0.992
2230	0.123	-0.156	1.110
2231	0.104	0.416	1.021
2240	0.258	-1.913	1.349
2250	0.124	0.230	1.049
2251	0.108	0.394	1.025
2260	0.134	0.499	0.999
2270	0.119	0.570	0.985
Calm water	0.155	0.516	1.030

**Table D.0.2** The results of interpolated propulsive factors for ducted propeller at

$$F_n = 0.14$$

ducted prop $F_n=0.14$	t	w	$\eta_r$
2100	0.151	0.644	0.960
2110	0.159	0.502	1.001
2120	0.165	0.655	0.942
2130	0.192	0.282	1.080
2140	0.317	-0.867	1.399
2150	0.190	0.515	1.001
2160	0.200	0.639	0.960
2170	0.190	0.632	0.989
Calm water	0.179	0.552	1.010

**Table D.0.3** The results of interpolated propulsive factors for ducted propeller at  $F_n = 0.20$

ducted prop @ $F_n=0.20$	t	w	$\eta_r$
2001	0.168	0.414	0.999
2010	0.252	-0.128	1.118
2011	0.157	0.340	1.001
2020	0.182	0.146	1.044
2021	0.169	0.406	0.987
2030	0.262	-0.640	1.264
2031	0.201	0.123	1.056
2040	0.213	-0.662	1.226
2050	0.247	0.111	1.037
2060	0.200	0.364	0.986
2070	0.198	0.410	0.990
Calm water	0.149	0.389	0.997

**Table D.0.4** The results of interpolated propulsive factors for open propeller at  $F_n = 0.20$

open prop @ $F_n=0.20$	t	w	$\eta_r$
2300	0.141	0.456	0.980
2310	0.089	0.385	0.990
2320	0.122	0.457	0.978
2330	0.128	0.144	1.022
2332	0.127	-0.290	1.078
2333	0.149	-0.370	1.088
2334	0.110	-0.326	1.083
2340	0.100	-0.601	1.103
2350	0.139	0.206	1.014
2360	0.125	0.416	0.985
2370	0.134	0.460	0.985
Calm water	0.159	0.312	1.025

To make correction for interpolated results the new data which is based on maximum recorded RPS from the experiments are presented as

**Table D.0.5** and **Table D.0.6**

**Table D.0.5** The corrected results of propulsive factors at  $F_n = 0.14$ 

test no.	t	w	$\eta_r$
2210	0.184	0.473	1.001
2230	0.156	0.480	1.000
2240	0.295	0.453	0.999
2250	0.140	0.486	1.001
2130	0.206	0.544	0.980
2140	0.326	0.517	0.989

**Table D.0.6** The corrected results of propulsive factors at  $F_n = 0.20$ 

test.no	t	w	$\eta_r$
2330	0.140	0.258	1.009
2332	0.142	0.277	1.007
2333	0.175	0.272	1.008
2334	0.124	0.266	1.008
2340	0.126	0.240	1.008
2010	0.368	0.292	0.999
2020	0.149	0.312	1.001
2030	0.408	0.288	1.009
2031	0.208	0.326	0.998
2040	0.252	0.301	0.986
2050	0.230	0.302	0.982